AD-776 763

ADVANCED EJECTOR THRUST AUGMENTATION STUDY-MASS ENTRAINMENT OF AXISYMMETRIC AND RECTANGULAR FREE JETS

William Peschke

Bell Aerospace Company

Prepared for:

Air Force Flight Dynamics Laboratory

April 1973

DISTRIBUTED BY:

NTIS

National Technical Information Service
U. S. DEPARTMENT OF COMMERCE
5285 Port Royal Road, Springfield Va. 22151

AD776768

AFFDL-TR-73-55

ADVANCED EJECTOR THRUST AUGMENTATION STUDY – MASS ENTRAINMENT OF AXISYMMETRIC AND RECTANGULAR FREE JETS

WILLIAM PESCHKE
BELL AEROSPACE DIVISION OF TEXTRON
P.O. Box 1
Buffalo, N.Y. 14240

TECHNICAL REPORT AFFDL-TR-73-55

APRIL 1973

DDC
RECEIVED
APR 8 1974

Approved for Public Release; Distribution Unlimited

AIR FORCE FLIGHT DYNAMICS LABORATORY
AIR FORCE SYSTEMS COMMAND
WRIGHT-PATTERSON AIR FORCE BASE, DAYTON, OHIO

Reproduced by
NATIONAL TECHNICAL
INFORMATION SERVICE
U S Department of Commerce
Springfield VA 22151

Unclassified

Security Classification

DOCUMENT CONTROL DATA - R & D

(Security classification of title, body of abstract and indexing annotation must be entered when the overall report is classified)

1. ORIGINATING ACTIVITY (Corporate author)

Bell Aerospace Company
P.O. Box 1, Buffalo, New York 14240

2a. REPORT SECURITY CLASSIFICATION

Unclassified

2b. GROUP

3. REPORT TITLE

Advanced Ejector Thrust Augmentation Study - Mass Entrainment of Axisymmetric and Rectangular Free Jets

4. DESCRIPTIVE NOTES (Type of report and inclusive dates)

Final Report - June 1972 thru April 1973

5. AUTHOR(S) (First name, middle initial, last name)

Peschke, William

6. REPORT DATE	7a. TOTAL NO. OF PAGES	7b. NO. OF REFS
April 1973	56	8

8a. CONTRACT OR GRANT NO.	9a. ORIGINATOR'S REPORT NUMBER(S)
F33615-72-C-2045	
b. PROJECT NO. 6813	
c.	9b. OTHER REPORT NO(S) (Any other numbers that may be assigned this report)
d.	AFFDL-TR-73-55

10. DISTRIBUTION STATEMENT

Approved for Public Release; Distribution Unlimited

11. SUPPLEMENTARY NOTES	12. SPONSORING MILITARY ACTIVITY
	Air Force Aerospace Research Laboratory

13. ABSTRACT

An experimental investigation has been performed to evaluate the entrainment characteristics of non-axisymmetric (rectangular) primary nozzles for ejector application. Data are presented which show the variation in mass entrainment rates of various nozzles as related to isentropic nozzle exit velocity and distance downstream of the nozzle exit. The entrained mass flow is determined by direct measurement for an axisymmetric nozzle and for rectangular nozzles with aspect ratios of 1, 10, 25, and 50.

Most of the data presented is for isentropic nozzle exit Mach numbers between about 0.08 and 0.5. Some data are presented for Mach numbers up to about 0.52. All data are for nozzles exhausting into quiescent atmosphere.

In contrast with results obtained for axisymmetric and square nozzles, the entrainment rates measured for jets produced by rectangular nozzles show a general increase with increasing Reynolds number, up to a Reynolds number between 1.0 and 2.0 x 10^4.

The experimental data show conclusively that primary air nozzles with large aspect ratios entrain more air than circular or square nozzles of equal cross-sectional area, with each nozzle providing its own "signature" for mass entrainment rate.

The same direct measuring technique is used for the measurement of mass entrainment by a multiple, alternating rectangular orifice *(hypermixing)* nozzle.

The results of these experiments indicate that the AFARL-developed hypermixing nozzle provides about 140 percent greater mass entrainment than an equivalent aspect ratio single nozzle, within ten inches of the nozzle exit.

It is shown that in the similarity region, for all single rectangular nozzles tested, the mass entrainment rate may be expressed in terms of axis velocity decay by a single equation of the form, $M = KU^{-1}$.

DD FORM NOV 1473

Unclassified

Security Classification

ia

Reproduced by
NATIONAL TECHNICAL
INFORMATION SERVICE
U S Department of Commerce
Springfield VA 22151

67

14 KEY WORDS	LINK A		LINK B		LINK C	
	ROLE	WT	ROLE	WT	ROLE	WT
Axisymmetric Free Jets						
Rectangular Free Jets						
Mass Entrainment						
Hypermixing Nozzles						

NOTICE

When Government drawings, specifications, or other data are used for any purpose other than in connection with a definitely related Government procurement operation, the United States Government thereby incurs no responsibility nor any obligation whatsoever; and the fact that the government may have formulated, furnished, or in any way supplied the said drawings, specifications, or other data, is not to be regarded by implication or otherwise as in any manner licensing the holder or any other person or corporation, or conveying any rights or permission to manufacture, use, or sell any patented invention that may in any way be related thereto.

Copies of this report should not be returned unless return is required by security considerations, contractual obligations, or notice on a specific document.

ADVANCED EJECTOR THRUST AUGMENTATION STUDY - MASS ENTRAINMENT OF AXISYMMETRIC AND RECTANGULAR FREE JETS

WILLIAM PESCHKE

Approved for Public Release; Distribution Unlimited

id

FOREWORD

This report describes work performed in the Research Department of Bell Aerospace Company for the U. S. Air Force Aerospace Research and Flight Dynamics Laboratories under Contract F33615-72-C-2045 (Project 6813 - Advanced Ejector Thrust Augmentation Study) in support of the laboratories' advanced ejector programs.

Advice and assistance during the course of these experiments were provided by Dr. Brian Quinn (AFARL), Mr. Carl Simmons (AFFDL), and Drs. S.W. Zelazny and J.H. Morganthaler and Mr. G. Salter of Bell Aerospace. Thanks are also due Messrs. B. Okulewicz and L. Golaschlag for their assistance in the reduction of the data obtained.

This technical report has been reviewed and is approved.

Leland M. Nicolai, Major USAF
Chief, Advanced Concepts Branch
Air Force Flight Dynamics Laboratory

CONTENTS

Pages iii and iv blank

ILLUSTRATIONS

ILLUSTRATIONS

TABLES

NOMENCLATURE

A	Cross-sectional area, sq. in.
C	Entrainment coefficient
C_D	Discharge coefficient, $\frac{m_o}{m_{otheo}}$
d	Minimum nozzle exit dimension, in.
l	Maximum nozzle exit dimension, in.
M	Mach number
m	$m_s + m_o$, total jet flow rate, lb/sec
m_o	Nozzle (primary) mass flow rate, lb/sec
m_s	Secondary (entrained) mass flow rate, lb/sec
m_s/m_o	Entrainment ratio
m/m_o	$1 + m_s/m_o$, entrainment rate
Re_d	Reynolds number based on d
U	Velocity in x (axial) direction, ft/sec
U_c	Jet centerline velocity, ft/sec
U_{oc}	Nozzle exit velocity, ft/sec
x	Axial distance from nozzle exit plane, in.
$\bar{x}$	x/d
ρ	Gas (air) density, lb/ft^3

I. INTRODUCTION

The specific objective of the experimental program discussed herein is to measure the mass entrainment of free, turbulent air jets produced by single and multiple nozzles using a direct measuring technique. The determination of entrainment rates for these nozzles will thus provide guidance for the design of ejector thrust augmentation systems.

Certain properties of free jet flows, regardless of their initial geometry, are characteristic of the processes occurring in an ejector. The jet flow becomes completely turbulent a short distance from the nozzle exit. As a result of the viscous effects, the jet becomes partly mixed with the surrounding fluid. So, parts of the surrounding medium are carried away (entrained) by the jet so that the mass flow within the jet increases in the downstream direction. Concurrently, the jet spreads and its velocity decreases, while the total momentum remains constant.

In the ejector, the primary jet flow induces flow in the adjacent stagnant region, lowering the static pressure, resulting in entry of secondary fluid into the ejector inlet. The rate of induction of secondary air (i.e., the entrainment rate) is a function of the pressure difference generated in the region between the primary jet flow and the ejector shroud, and consequently, on the turbulent mixing of the primary jet flow with the ingested air.

The performance of an ejector is influenced by a number of variables. These include the inlet shape, the inlet/primary nozzle and inlet/diffuser area ratios, diffuser length and shape, and primary flow nozzle geometry.

The primary flow nozzle in an ejector designed for cold thrust augmentation (CTA) must similarly exhibit certain characteristics. It must efficiently produce thrust by itself, entrain substantial amounts of secondary air within a minimum streamwise distance and as part of the ejector, must exhibit minimum energy dissipation during the mixing process to provide maximum thrust augmentation. It is toward the second requirement that the present investigation is directed.

Evidence in the literature indicates that significant increases in mass entrainment can be obtained through proper design of the primary nozzle. In particular, the work done by Trentacoste and Sforza (Reference 1) showed that increases in entrainment rates of 10 percent or more can be anticipated for a rectangular slot (L/d = 10), as compared with an axisymmetric jet. Earlier experimental work by Tuve, et al (Reference 2) provided indications that an increase in aspect ratio, L/d from 1 (square nozzle) to 24 (rectangular slot of area equal to square nozzle) could increase the entrainment rate by as much as 35 percent. (Based on the data given in this Reference, the Reynolds numbers computed for these configurations were in the range, 0.6 to 15.0 x 10^4.) In addition, an increase in entrainment rate for an axisymmetric jet was observed by Ricou and Spalding (Reference 3) when the primary flow Reynolds number (based on nozzle exit diameter) is less than 2.5 x 10^4

In order to adequately assess the rate at which the secondary air is entrained, previous work (specifically with axisymmetric primary nozzles) has centered on the determination of radial velocity profiles, u (y) at a number of axial locations, x, measured from the primary nozzle exit. The axial increase in the total mass flow rate is a measure of the entrainment rate of the primary jet. The total mass flow rate, m, across any section is obtained through an integration over the section.

$$m = 2\pi \int_0^\infty \rho\, u(y)\, y\, dy$$

where ρ is the gas density. Although this procedure by virtue of its simplicity, is attractive, it suffers from uncertainty in the measurement of ρ u at larger values of y where u is small and the flow may not be steady. In the non-axisymmetric case, the flow asymmetry and non-uniformity make it necessary to probe the entire flow field to estimate the mass entrainment. The determination of the mass entrainment for two or more jets in close proximity requires a similar procedure.

The non-circular primary jets are of significance since it has been indicated (References 1, 2) that increases in mass entrainment by a primary nozzle are obtainable through proper design of the nozzle geometry.

This report deals specifically with the results of direct measurements of the mass entrainment rates of various nozzles appropriate for ejector application.

The method developed by Ricou and Spalding (Reference 3) was used to obtain the data reported herein. Single axisymmetric and rectangular nozzles (aspect ratios = 1, 10, 25 and 50) and a multiple, alternating rectangular orifice *(hypermixing)* nozzle developed by the Air Force Aerospace Research Laboratory for CTA application were tested in this investigation.

II. DESCRIPTION OF EXPERIMENT

A schematic of the experimental apparatus used for the measurement of the mass entrainment of primary nozzles is shown in Figure 1. The method of measurement involves exhausting a primary nozzle flow into a chamber as shown. The porous wall permits the distribution of a controlled and measured amount of fluid to flow through it in a radially inward direction. When this secondary flow, entrained by the primary jet flow, is equal to that which the primary jet would entrain when exhausting into a stationary, ambient fluid, the axial pressure gradients in the flow disappear.

The geometric axes of the test nozzles are coincident with the axis of the cylindrical porous wall. With the exception of the nozzle exit orifice, the base of this cylinder is completely closed. The upper (exit) end of the cylindrical extrainment chamber thus formed is partially closed by an exit aperture which is carefully sized so as not to interfere with the jet or secondary flow in the chamber.

The flow area between the porous wall and the outer cylinder is specified so as to provide an initial velocity at the entrance to this annulus of 5 ft/sec at maximum flow. The axial pressure variation in the outer chamber is thus minimized and indeed, the maximum axial pressure differential measured is 0.20 in. of water.

To achieve a pressure differential of about 0.25 psi across the porous wall (to ensure uniform flow through the porous wall) at maximum secondary flow, a flow resistance of about 100 rayls[1] is required. Based on work performed previously by the author in (Reference 4), two layers of dacron crepe fabric provide a flow resistance of this magnitude, where the radial velocity through the porous wall is limited to about 3 ft/sec.

Direct reading calibrated flowrators were used to measure the primary and secondary air flow rates. Pressure transducers and thermocouples were used in conjunction with the flow meters to correct the readings to standard conditions.

The axial pressure difference measured is that across the exit aperture with respect to atmospheric pressure. A Kistler 314D differential servo pressure transducer was used to sense this quantity. It is worth noting that this sensing system must be capable of resolving pressure differentials of less than 0.001 in. of water. Significant scatter in preliminary data was attributed to a null shift in the transducer output (read on the display of a digital voltmeter) induced by vibration and thermal transients. The problem was eliminated by isolating the transducer, thermally and mechanically from the laboratory environment. The resolution of the transducer system was assessed to be on the order of 0.0002 in. of water.

The pressure transducer was connected to the exit aperture pressure taps through a manual pressure scanner. This permitted sensing any one of several pressure taps in the exit aperture plate, providing an assessment of the circumferential pressure distribution at the exit aperture. No pressure differences between these taps were noted during the tests. The use of the scanner also permitted checking of the transducer null output during a test.

Some of the data scatter recorded in the preliminary tests could be attributed to interference by the exit aperture plate with the axial flow through the extrainment chamber. Appendix A describes the tests performed to investigate appropriate aperture dimensions for the entrainment tests.

In order to facilitate the reduction of test data, a computer program was written. Descriptions of the nomenclature and coding are presented in Appendix B, along with examples of the input/output.

---

[1] Flow resistance in rayls, $R = \Delta P/U$, where ΔP = pressure differential, U = upstream velocity.

III. EXPERIMENTAL RESULTS

One axisymmetric and four rectangular single nozzles were tested to determine their entrainment characteristics as functions of (a) nozzle exit velocity, U_{oc} and (b) axial distance, x measured from the nozzle exit plane. This constituted the first phase of the test program. The axisymmetric nozzle diameter, d is 0.480 inch, and the aspect ratios, L/d of the rectangular nozzles are 1, 10, 25, and 50. The cross-sectional area of all the single nozzles is 0.1809 sq. in. Diagrams of the nozzles are shown in Figures 2 to 6, inclusive. A tabulation of the test conditions is presented in Table I. The nozzle with an aspect ratio of 5 was fabricated but not tested since the data acquired for the four rectangular nozzles gave an adequate representation of the required data.

The second phase of the test program involved testing of an AEDC-supplied alternating orifice ("hypermixing") nozzle (Reference 5) to assess its entrainment characteristics. The aspect ratio of each orifice of this nozzle is approximately 2.3. Entrainment data were acquired with two and four orifices, characterized by effective aspect ratios of 4.6 and 9.2, respectively. The cross-sectional area of each orifice is 0.0562 sq. in. A diagram of the nozzle is shown in Figure 7 and a tabulation of the test conditions for this nozzle is presented in Table II.

For each test, data were acquired to provide information for the evaluation of discharge coefficients. These data are plotted in Figure 8.

A. AXISYMMETRIC NOZZLE

Results of tests with the axisymmetric nozzle are shown in Figure 9. The mass entrainment ratio at each axial distance from the nozzle exit is constant over the Reynold's number range considered. The data are also presented to show the axial variation in entrainment ratio in Figure 10. Both of these results are qualitatively consistent with the conclusions of Ricou and Spalding (Reference 3) for axisymmetric turbulent jets. Noting that the total mass flow rate past any station, x downstream of the nozzle exit plane is the sum of the primary and secondary flows, Ricou originates the entrainment rate, $m/m_o = 1 + m_s/m_o$ and indicates that the entrainment rate in the region of linear axis velocity decay ($U_o/U_{oc} \sim x^{-1}$) of the axisymmetric jet may be described by the equation,

$$\frac{m}{m_o} = C\left(\frac{x}{d}\right)$$

where m = total mass flow = $m_s + m_o$, m_s = secondary mass flow, m_o = primary mass flow, x = axial distance from nozzle exit plane, and d = the nozzle exit diameter. Ricou and Spalding cited a value, C = 0.32. The data obtained from the present work are presented in a similar manner in Figure 11. The slope of the data shown for $x/d_o \geq 13$ is C = 0.35. The disagreement with Reference 3 might be attributed to differences in primary nozzle configuration which affects initial turbulence levels and discharge coefficients.

The data presented for the minimum axial distance, x/d = 4.3 show that the entrainment in this region is greater than can be described by the Ricou-Spalding relationship. Note that this axial location is less than the length of the potential core for an axisymmetric jet. Data obtained here can be compared with the results of Hill (Reference 6) who has done the only definitive investigation of local entrainment rate of axisymmetric air jets. At an average distance, x/d = 2.1, Hill obtains a value of the entrainment coefficient, C = 0.18. The present work indicates a value, C = 0.22 for the average slope between x/d = 0 and x/d = 4.3. This is in fair agreement with the previously obtained result, and as discussed above, might be due to differences in initial conditions.

B. 1:1 ASPECT RATIO NOZZLE

The mass entrainment of the square (aspect ratio = 1) nozzle is less than the entrainment measured for the axisymmetric nozzle. Data obtained at four axial distances from the nozzle exit plane indicate a behavior similar to that noted for the axisymmetric nozzle. That is, the entrainment ratio, m_s/m_o is constant at any axial station over the test range of Reynolds numbers. The data presented in Figure 12 thus can be recast to show the variation of entrainment rate as a function of x/d measured from the nozzle exit plane, shown in Figure 13. The normalizing dimension, d = 0.42 in. is the width of the square nozzle exit.

The entrainment coefficient, C = 0.33 for x/d between 14.66 and 35.55 (6.25 and 15.10 inches, respectively from the nozzle exit plane). This value agrees reasonably well with the value, C = 0.35 obtained for the axisymmetric nozzle.

C. 10:1 ASPECT RATIO NOZZLE

In contrast with the results obtained for the axisymmetric and square nozzles, the entrainment ratios measured for the jets produced by the rectangular nozzles show a general increase with increasing Reynolds number, up to a Reynolds number between 1.0 and 2.0 x 10^4. The Reynolds number in each case is based on the minimum dimension, d of each nozzle, indicated in Table I.

The entrainment ratio data acquired for the 10:1 aspect ratio nozzle are presented for the Reynolds number range, 0.6 to 2.3 x 10^4 in Figure 14. The entrainment ratios obtained from these measured data at nozzle exit velocities, U_{oc} = 100, 200, and 300 ft/sec are plotted for each axial station, x/d in Figure 15.

D. 25:1 ASPECT RATIO NOZZLE

Data were obtained for both the 25:1 and 50:1 aspect ratio nozzles at isentropic nozzle exit velocities ranging between 100 and 500 ft/sec.

The entrainment ratio data for the 25:1 aspect ratio nozzle are provided in Figure 16. A Reynolds number range, 0.4 to 2.0 x 10^4 is covered in the data acquired at x/d values of 73.5 and 118. These results indicate that the rate of increase in entrainment ratio with increasing Reynolds number diminishes as the Reynolds number exceeds about 1.5 x 10^4. The determination of the nozzle exit velocity which gives maximum entrainment appears to be a worthwhile subject for additional investigation.

The axial variation in entrainment rate for the 25:1 aspect ratio nozzle is presented in Figure 17 for isentropic nozzle exit velocities, U_{oc} = 100, 200, and 300 ft/sec.

E. 50:1 ASPECT RATIO NOZZLE

The final configuration tested in the single nozzle series was characterized by an aspect ratio of 50:1. As in the tests with the 25:1 aspect ratio nozzle, data were obtained for isentropic nozzle exit velocities exceeding 500 ft/sec at two axial locations. These data shown in Figure 18 indicate a decrease in the rate of change of entrainment ratio for a Reynolds number between 1.0 and 1.2 x 10^4. The measured entrainment ratios at each axial location increase as the nozzle exit Reynolds number increases from about 0.3 to 1.0 x 10^4.

Entrainment ratios obtained from these data at nozzle exit velocities, U_{oc} = 100, 200, and 300 ft/sec are plotted as a function of distance from the nozzle exit plane in Figure 19.

4 ALTERNATING ORIFICE (HYPERMIXING) NOZZLE

Due to the uncertainty in the spreading rate of the jet flow generated by the hypermixing nozzle, investigations with this nozzle were limited to tests with four of the ten 0.156 x 0.36 orifices. The central two orifices were tested first at one axial length by covering all but these with a sealing tape. At the same distance from the nozzle exit, the tape was removed from the adjacent orifices to obtain data for four orifices.

The tests were limited also, in the sense that only two axial lengths of the entrainment chamber could be used due to the length (5.25 in.) of the nozzle assembly.

The data presented in Figures 20 and 21 show the entrainment ratios measured for the two and four orifice configurations, respectively.

Lower entrainment ratios were measured for the four orifice tests at the maximum length tested, x = 9.85 inch, than were measured for the two-orifice configuration at this length. It is concluded that the largest exit aperture plate, corresponding to an aperture angle of 48° degrees with respect to the nozzle center line, was inadequate to provide valid data. The solution to this problem, as used successfully in Reference 3, is to extend the entrainment chamber, using a larger diameter porous cylinder for the extension.

The data for the two-orifice configuration are limited in extent since only two entrainment lengths could be considered due to the limitation imposed by the nozzle length. However, as will be discussed subsequently, the data are consistent with the single nozzle results.

Comparison of the data at x = 4.75 inch presented in Figures 20 and 21 show that the entrainment ratios for the two and four orifice configurations are equal.

IV. ANALYSIS OF RESULTS

A. DISCUSSION OF DATA

The axial variation in mass entrainment rate has been plotted for nozzle exit velocities, U_{oc} = 100, 200, and 300 ft/sec in Figures 22 to 24 for each nozzle considered in this investigation. Hypermixing nozzle results for U_{oc} = 100 ft/sec were obtained from a linear extrapolation of the acquired data.

The results provide a clear indication of the relative entrainment rates of the single nozzles tested and of the alternating orifice (hypermixing) nozzle. Of the single nozzles (all of which are of equal area), the nozzle with an aspect ratio of 50 entrains the maximum secondary flow in a minimum distance. The hypermixing nozzle on the other hand provides substantially greater entrainment, that is, 67 percent more than the 50:1 aspect ratio single nozzle at a distance of 10 inches from the nozzle exit plane. The aspect ratio of each hypermixing nozzle orifice is L/d = 2.3. It may be conjectured that an increase in this aspect ratio would provide even greater entrainment rates.

The variation in entrainment rate, m/m_o as a function of aspect ratio determined from the data obtained is shown in Figure 25. The advantage of the greater aspect ratio is emphatically displayed, providing at least 10 percent more entrainment than the square nozzle at the same axial distance (x = 15.10 in.) from the nozzle exit. Closer to the nozzle exit (x = 2.06 in.) a 60 percent increase is noted. The increase in entrainment ratio as the velocity is increased from 100 to 300 ft/sec is no more than 8 percent, the maximum value attained with the nozzle of aspect ratio equal to 50.

As will be demonstrated subsequently, the relationship between the entrainment rates of the various nozzles are predictable on the basis of their respective axis velocity decay rates.

B. DATA CORRELATION

A correlation between the experimental data obtained in this program and published data (Reference 7) for axis velocity decay for various jets has been achieved. Referring to the data in Figures 26, 27, and 28, the entrainment rate, $M = m/m_o$ can be expressed in terms of axial distance from the nozzle exit plane, $\bar{x} = x/d$ by the general expression,

$$M = a\,\bar{x}^{q} \tag{1}$$

where a and q are to be determined. Velocity decay data presented in Figure 29 (Reference 7) can also be expressed generally by an expression of the form,

$$\frac{U_c}{U_{oc}} = \bar{U} = b\,\bar{x}^{n} \tag{2}$$

for the faired curves shown. (The points shown in Figure 29 indicate those values of $\bar{x}$ where entrainment data were obtained.) Values of the coefficients a, b and exponents q, n derived from these data are tabulated in Table III. The value of the exponent, n is, of course, -1.0 for those sections of the velocity decay curves lying in the similarity or axisymmetric decay regions.

Substitution of the expressions for $\bar{x}$ obtained from Eq (2) into Eq (1) provide relationships for mass entrainment rate, M as a function of axis velocity, U in the form,

$$M = a\left[\left(\frac{D}{b}\right)^{\frac{q}{n}}\right] \tag{3}$$

or $$M = K\,\bar{C}^{P} \tag{4}$$

Values of the coefficient, K and exponent, P are also presented in Table III.

Inasmuch as axis velocity decay data for nozzle exit aspect ratios of 25 and 50 are not available, the data for aspect ratios of 20 and 40 were used. The agreement between the generated expressions and the experimental data is surprisingly good in the axisymmetric decay region.

The correlation was performed for three of the test nozzle exit velocities, U_{oc} = 100, 200, and 300 ft/sec. Examination of the constants in Table II shows that the variation of the constants between 100 and 300 ft/sec for a given nozzle is not substantial. An average value selected for engineering evaluations should generally prove adequate for estimates of entrainment rates.

An appropriate average value of the exponent, P for the axisymmetric, square, and 10:1 aspect ratio nozzle appears to be -1.20. Since axis velocity decay data specifically for 25:1 and 50:1 aspect ratio nozzles are not available, the values of P for these two nozzles must be considered tentative. Equations for mass entrainment by the former three nozzles then may be written as follows:

(a) Axisymmetric nozzle,

$$\frac{m}{m_o} = 1.726\left(\frac{U_c}{U_{oc}}\right)^{-1.20} \qquad 8.7 \leq \bar{x} \leq 31.45 \tag{5}$$

(b) Square nozzle,

$$\frac{m}{m_o} = 1.377\left(\frac{U_c}{U_{oc}}\right)^{-1.20} \qquad 9.6 \leq \bar{x} \leq 35.55 \tag{6}$$

(c) 10:1 Aspect ratio nozzle,

$$\frac{m}{m_o} = 1.505\left(\frac{U_c}{U_{oc}}\right)^{-1.20} \qquad 4.45 \leq \bar{x} \leq 112 \tag{7}$$

Consideration of all values of P suggests that for values of $\bar{x} \geq 100$, the exponent P approaches a value of -1.0. Based on this assumption, a common equation for all rectangular nozzles (including the square) may be written as follows:

$$\frac{m}{m_o} = 1.78\left(\frac{U_c}{U_{oc}}\right)^{-1} \qquad \bar{x} \geq 100 \tag{8}$$

whereas the entrainment rate for the circular nozzle is

$$\frac{\dot{m}}{\dot{m}_o} = 2.4 \left(\frac{U_c}{U_{oc}}\right)^{-1} \qquad \bar{x} \geq 100 \tag{9}$$

Only fair agreement with the results of Ricou and Spalding (Reference 3) is obtained. It should be noted that for the expression developed by them, the values of the constants, a and m in Eq (3) are 0.32 and 1.0 respectively. This provides values for K and P of 2.205 and -1.0, which yield results that are in fair agreement with the present study.

The significant point to be made is that the axis velocity decay for various nozzle shapes can be considered to be a "Signature" for that nozzle. As a result, for any given nozzle shape, a specific set of constants should be adequate to describe the entrainment of the nozzle once the axis velocity decay, a relatively easily measured parameter, is known.

It is interesting to observe that the inflection points in the data shown in Figures 26 through 28 for the axisymmetric, square, and 10:1 aspect ratio nozzles generally coincide with the corresponding points in the axis velocity plot in Figure 29.

The data for the hypermixing nozzle as obtained from Figure 21 are plotted in Figures 27 and 28 for isentropic nozzle exit velocities, U_{oc} = 200 and 300 ft/sec. The aspect ratio of each orifice is 2.3 and the data appear to be consistent with the other measured results. On the basis of the acquired experimental data, the values of the coefficient, a,and exponent, q,were deduced and are presented in Table IV. For lack of axis velocity decay data, no expression for entrainment rate as a function of velocity decay can be derived.

V. CONCLUSIONS AND RECOMMENDATIONS

The results obtained from this investigation show conclusively that primary air nozzles with large aspect ratios entrain more air than circular or square nozzles of equal cross-sectional area. The largest aspect ratio (50:1) nozzle tested entrained 10 percent more secondary air than the equal area square nozzle at a point 15.10 inches downstream from the nozzle and 60 percent more at a distance of 2.06 inches.

Increasing flow velocity from 100 to 400 ft/sec induced an 8 percent increase in entrainment rate for the 50:1 aspect ratio nozzle. A further increase in velocity induced an additional increase, the maximum value of which was not determined as this was beyond the scope of the present program.

Based on the limited axis velocity data available for non-axisymmetric jets, the entrainment rates of single nozzles can be correlated empirically with axis velocity decay. Each nozzle, of different aspect ratio, provides its own "Signature" of mass entrainment, a characteristic of the axis velocity decay of that nozzle. Inflection points in the axial mass entrainment data for axisymmetric, square and 10:1 aspect ratio rectangular nozzles correspond quite well with inflection points in plots of axis velocity for these same nozzles.

The results of the tests with the axisymmetric nozzle are in disagreement (8.5 percent) with previously published data (Reference 3). It is conceivable that the upstream turbulence levels for the present nozzle and previously tested nozzles are sufficiently dissimilar to cause this discrepancy.

The tests with the alternating orifices (hypermixing) nozzle show that this nozzle induces the greatest secondary air flow of all nozzles tested: 67 percent more than the largest aspect ratio (50) nozzle at a distance of 10 inches. For CTA applications, the data acquired show that this nozzle is most appropriate of those tested. The limitation imposed by the size of the experimental facility prevented extensive testing of this nozzle. Based on the results of the investigation reported herein, the following recommendations are made:

1. Extend the investigations of hypermixing nozzles for larger entrainment lengths by extending the present entrainment chamber length. Obtain axis velocity decay data for this nozzle to provide data for entrainment prediction. As performed in the present study. Investigate the possibility of modelling the flow field using an appropriate computational method. (e.g. Ref. 8.)

2. Obtain entrainment rate data for a hypermixing nozzle with a single orifice aspect ratio greater than 2.3.

3. Obtain entrainment rate data for single nozzles and hypermixing nozzles for elevated temperature primary flow. Acquire entrainment data for nozzles with aspect ratios greater than 50 to determine if a maximum exists.

4. Determine the point of maximum entrainment for nozzles with aspect ratios of 10, 25, and 50 for nozzle exit Mach numbers greater than 0.3.

5. Examine the possibility of determining the entrainment rates of other primary nozzle geometries which will satisfy criteria for CTA and HTA applications.

6. Determine relative entrainment rates of separated and adjacent hypermixing orifice pairs.

7. Investigate the effects of varying the hypermixing nozzle orifice inclination with respect to the geometric axis of the nozzle.

VI. REFERENCES

1. Trentacoste, N., Sforza, P., "Further Experimental Results for Three-Dimensional Free Jets," AIAA Jnl., V. 5, No. 5, May, 1967.

2. Tuve, G.L., Priester, G. B., Wright, D. K., "Entrainment and Jet Pump Action of Air Streams," Heating, Piping, and Air Conditioning Jnl., 1942.

3. Ricou, F. D., Spalding, D. B., "Measurements of Entrainment by Axisymmetrical Turbulent Jets," Jnl. of Fluid Mechanics, V. 11, 21, 1961.

4. Tomboulian, R., "Research and Development of a Sonic Boom Simulation Device," (Final Report) NASA Contract No. NAS1-7985, GASL TR No. 713, November 1968.

5. EastDike, C.N., II, "The Macroscopic Characteristics of Some Subsonic Nozzles and the Three-Dimensional Turbulent Jets They Produce," USAF ARL Report 71-0058, March, 1971.

6. Hill, B. J., "Measurement of Local Entrainment Rate in the Initial Region of Axisymmetric Turbulent Air Jets," Jnl. of Fluid Mechanics, V. 51, part 4, 1972.

7. Steiger, M. H., Hinz, W., Sforza, P. M., and Trentacoste, N., "Studies in Three-Dimensional Free Mixing," AIAA Paper 65-49, AIAA 2nd Aerospace Sciences Meeting, 1965.

8 Baker, A.', and Zelazny, S W., A Theoretical Study of Mixing Downstream of Transverse Injection into a Supersonic Boundary Layer, NASA CR-112254, Dec. 1972. (Bell Aerospace Report 9500-920263)

TABLE I
SINGLE NOZZLE TEST CONDITIONS

Nozzle A.R.	d	x	$\frac{x}{d}$	U_{oc}	$Re_d \times 10^{-4}$
Axi.	0.480	2.06	4.30	89 - 342	1.99 - 7.60
		6.25	13.00	66 - 343	1.48 - 7.61
		10.00	20.85	91 - 338	2.02 - 7.52
		15.10	31.45	91 - 336	2.02 - 7.47
1:1	0.425	2.06	4.85	112 - 342	2.36 - 7.10
		6.25	14.66	86 - 342	1.82 - 7.20
		10.00	23.55	96 - 345	2.01 - 7.25
		15.10	35.55	94 - 346	1.86 - 6.72
10:1	0.1345	2.06	15.30	92 - 349	0.61 - 2.32
		6.25	46.40	81 - 344	0.54 - 2.29
		10.00	74.50	93 - 337	0.62 - 2.24
		15.10	112.00	93 - 338	0.62 - 2.25
25:1	0.085	2.06	24.25	96 - 341	0.38 - 1.34
		6.25	73.50	86 - 526	0.34 - 2.07
		10.00	118.00	98 - 354	0.39 - 1.97
		15.10	178.00	98 - 357	0.39 - 1.41
50:1	0.060	2.06	34.40	97 - 348	0.27 - 0.97
		6.25	104.00	76 - 575	0.21 - 1.60
		10.00	167.00	106 - 356	0.30 - 1.50
		15.10	251.00	105 - 352	0.29 - 0.98

A.R. = Nozzle Aspect Ratio, L/d

d = Minimum Nozzle Dimension, Inches

x = Entrainment Length, Inches

U_{oc} = Isentropic Nozzle Exit Velocity, ft/sec

Re_d = Reynolds Number Based on d.

TABLE II
HYPERMIXING NOZZLE TEST CONDITIONS

Aper.	d	x	$\frac{x}{d}$	U_{oc}	$Re_d \times 10^{-4}$
2	0.156	4.75	30.4	201 - 360	1.44 - 2.58
	0.156	9.85	63.1	202 - 362	1.45 - 2.59
4	0.156	4.75	30.4	196 - 361	1.43 - 2.63
	0.156	9.85	63.1	194 - 358	1.41 - 2.62

Aper. = No. of nozzle apertures

TABLE III

CONSTANTS FOR DETERMINATION OF MASS ENTRAINMENT OF SINGLE NOZZLES

Nozzle A. R.	U_{oc} ft/sec	$\bar{x}$ Range	a	q	b	n	K	P
Ax	100 - 300	4.3 – 8.7	0.722	0.566	1.47	0.26	1.66	2.16
		8.7 – 31.45	0.1695	1.20	6.90	-1.0	1.726	1.20
1.0	100 - 300	4.85 – 9.6	0.750	0.498	1.73	-0.37	1.98	1.32
		9.6 – 35.55	0.161	1.16	6.38	-1.0	1.38	-1.16
10	100	15.3 – 38.5	0.502	0.502	1.854	-0.314		
		38.5 –112.0	0.045	1.15	21.8	-1.0	1.61	-1.15
	200	15.3 – 41.0	0.47	0.579	1.854	-0.314		
		41.0 –112.0	0.038	1.20	21.8	-1.0	1.505	-1.20
	300	15.3 – 44.5	0.405	0.578	1.854	-0.314		
		44.5 –112.0	0.035	1.22	21.8	-1.0	1.50	-1.22
25	100	24.3 – 54.0	0.895	0.405	2.87	-0.505		
		54.0 –110.0	0.895	0.405	2.87	-0.505		
		110.0 –178.0	0.044	1.06	29.7	-1.0	1.59	-1.06
	200	24.3 – 58.0	0.561	0.449	2.87	-0.505		
		58.0 –110.0	0.049	1.044	2.87	-0.505		
		110.0 –178	0.049	1.044	29.7	-1.0	1.69	-1.04
	300	24.3 – 61.0	0.604	0.445	2.87	-0.505		
		61.0 –110.0	0.063	1.00	2.87	-0.505		-1.00
		110.0 –178.0	0.063	1.00	29.7	-1.0	1.87	-1.00
50	100	34.5 – 74.5	0.468	0.48	2.07	-0.45		
		74.5 –190.0	0.052	0.99	2.07	-0.45		
		190.0 –251.0	0.052	0.99	37.2	-1.0	1.855	-0.99
	200	34.5 – 78.0	0.465	0.488	2.07	-0.45		
		78.0 –190.0	0.056	0.98	2.07	-0.45		
		190.0 –251.0	0.056	0.98	37.2	-1.0	1.93	-0.98
	300	34.5 – 84.0	0.512	0.475	2.07	-0.45		
		84.0 –190.0	0.062	0.96	2.07	-0.45		
		190.0 –251.0	0.062	0.96	37.2	-1.0	1.97	-0.96

TABLE IV

CONSTANTS FOR DETERMINATION OF MASS ENTRAINMENT OF HYPERMIXING NOZZLE (TWO ORIFICES ONLY)

U_{oc} ft/sec	$\bar{X}$ Range	a	q
200	30.4-63	0.112	1.145
250	30.4-63	0.115	1.144
300	30.4-63	0.122	1.135
350	30.4-63	0.125	1.134

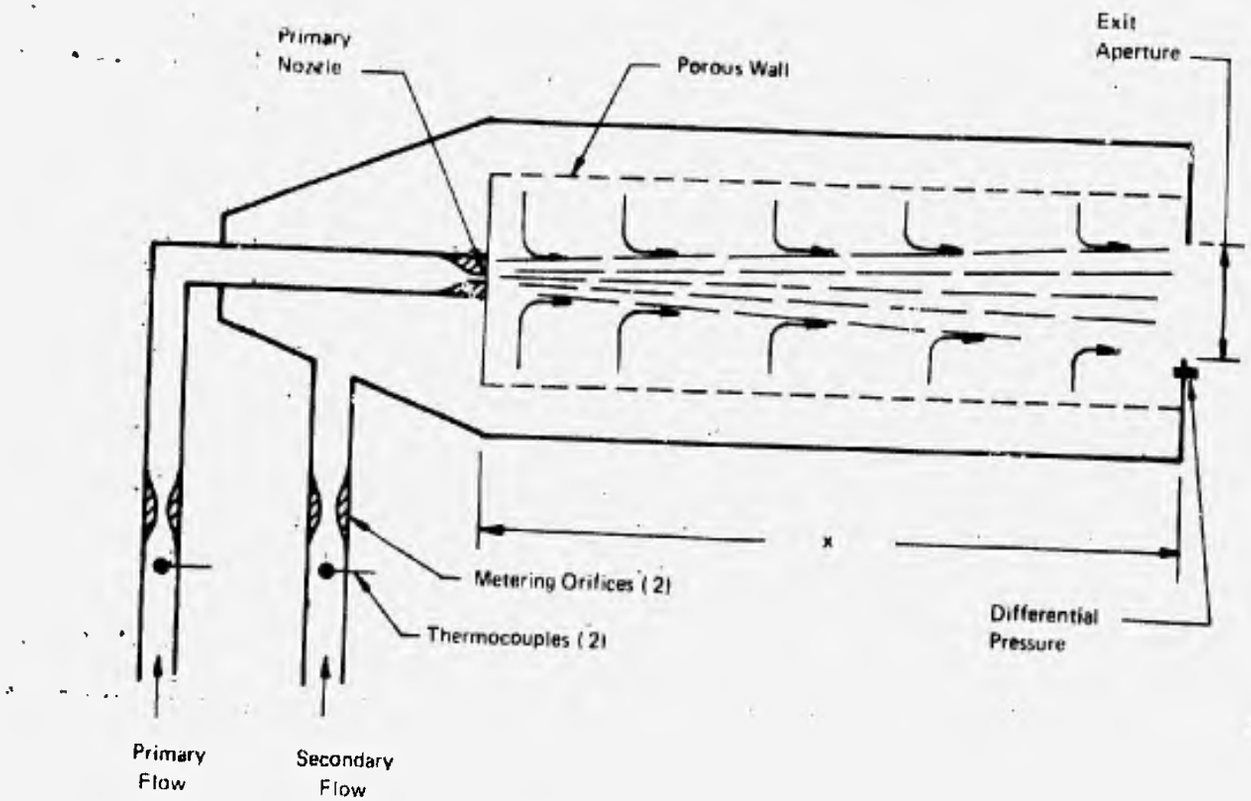

Figure 1. Mass Entrainment Measuring Device

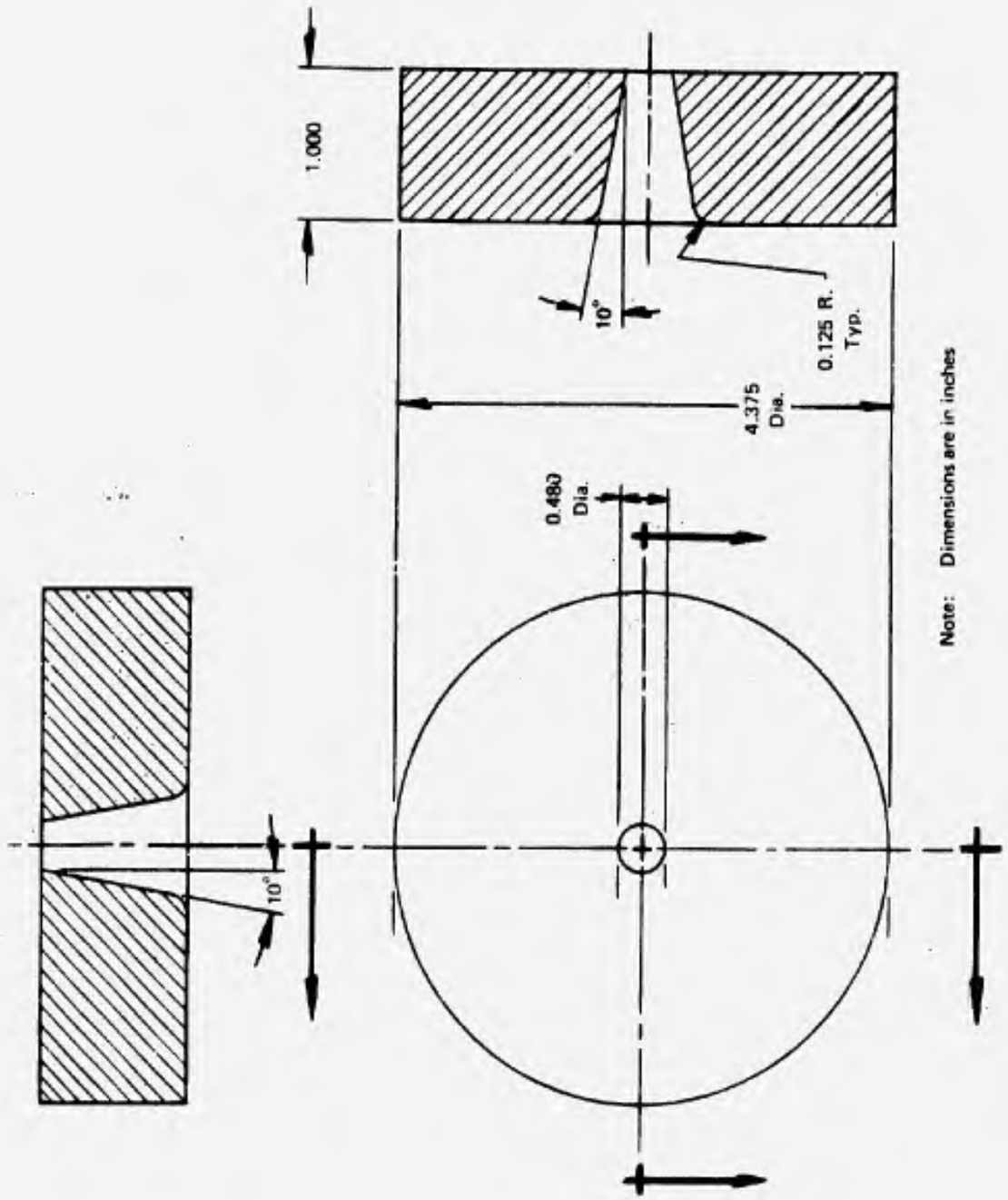

Figure 2. Axisymmetric Nozzle

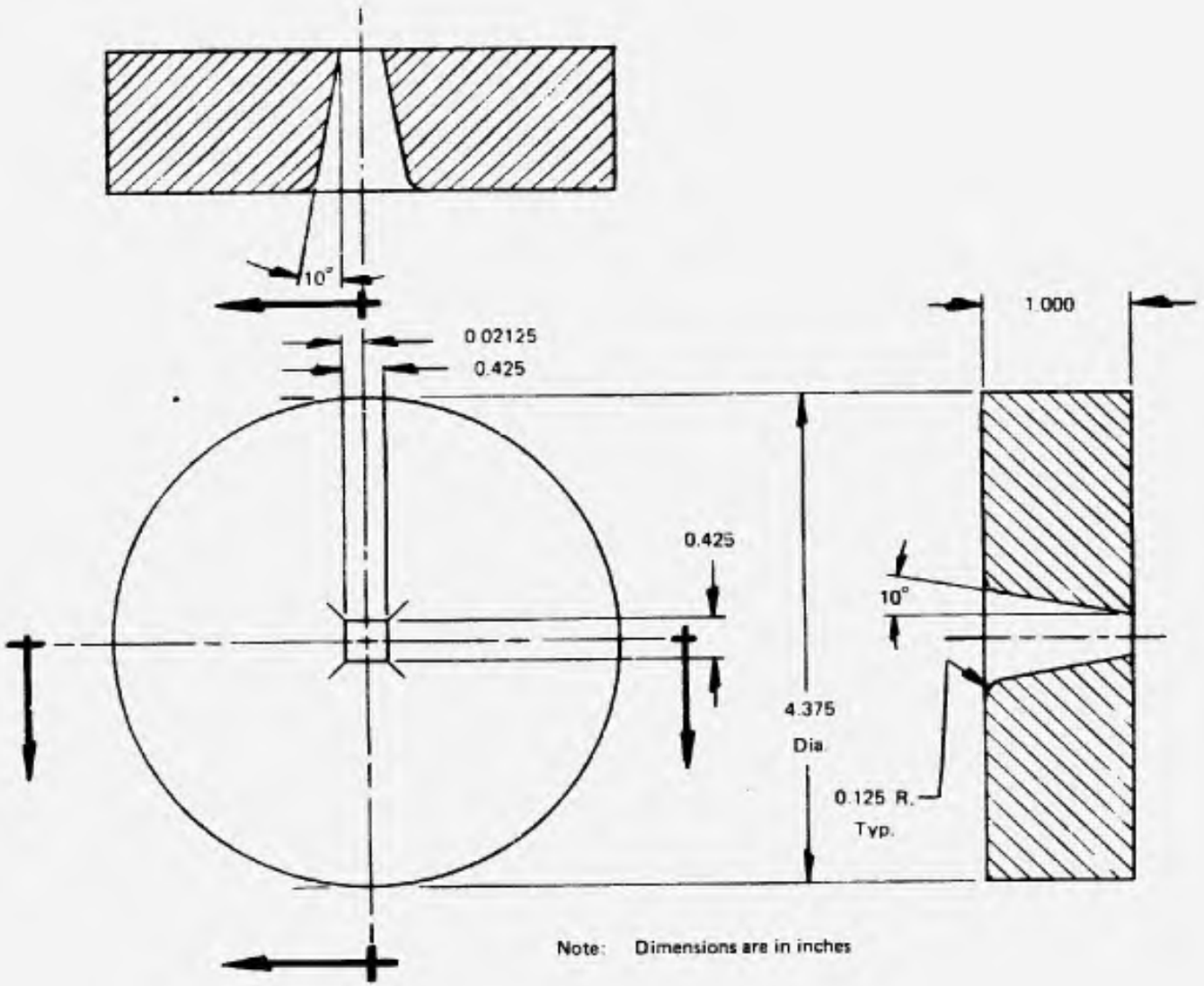

Figure 3. Square Nozzle (Aspect Ratio, L/d = 1.0)

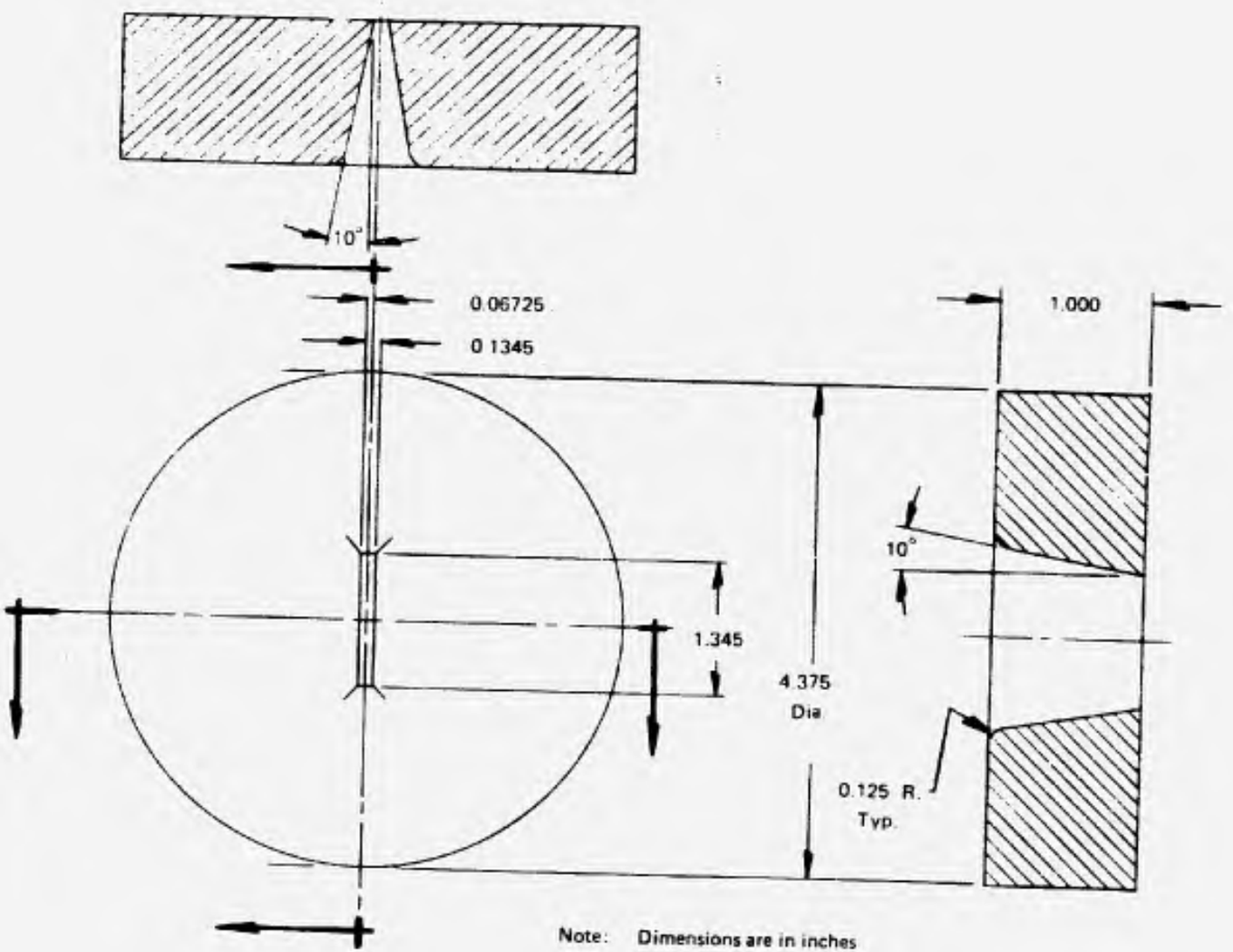

Figure 4. Rectangular Nozzle (Aspect Ratio, L/d = 10)

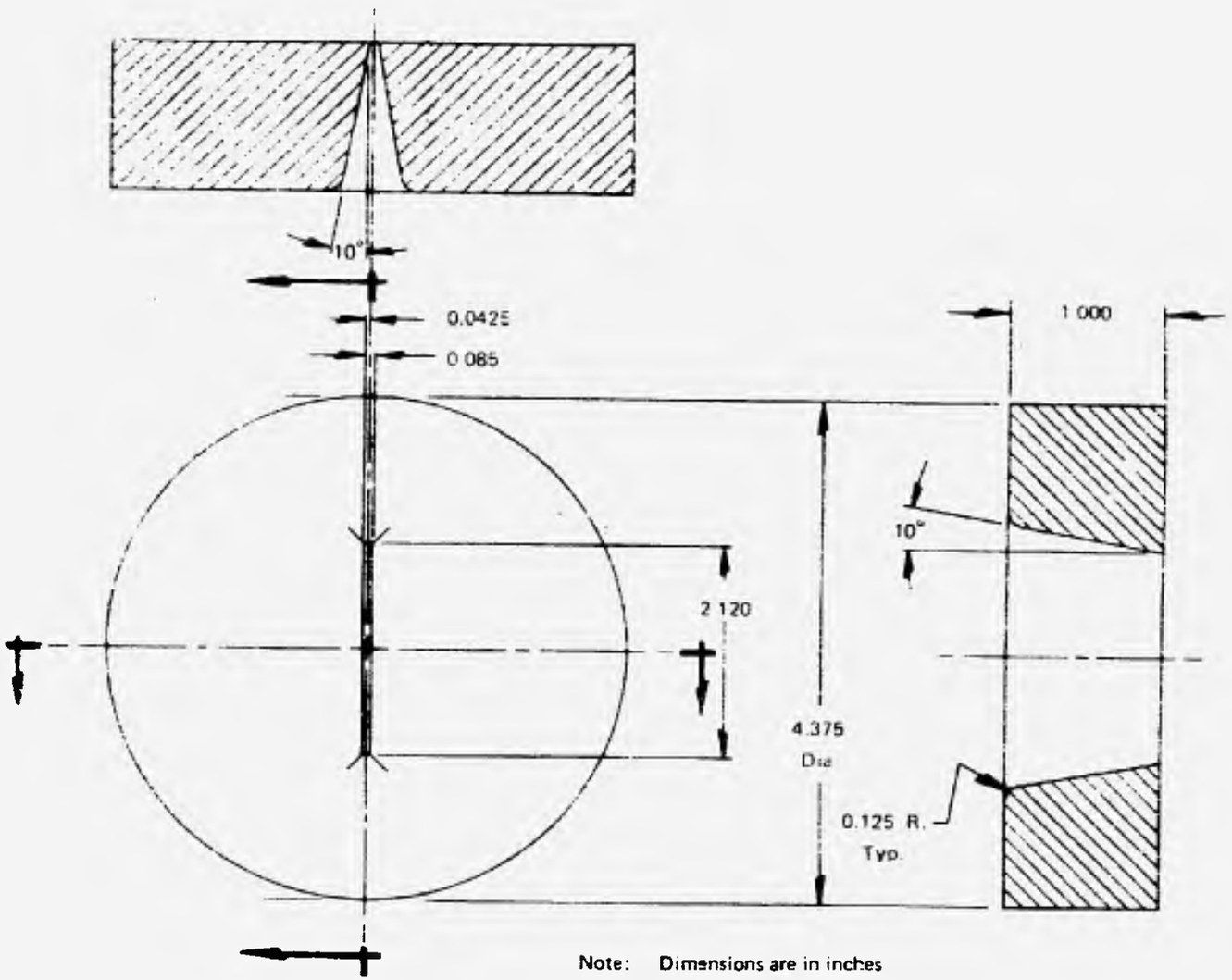

Figure 5. Rectangular Nozzle (Aspect Ratio, L/d = 25)

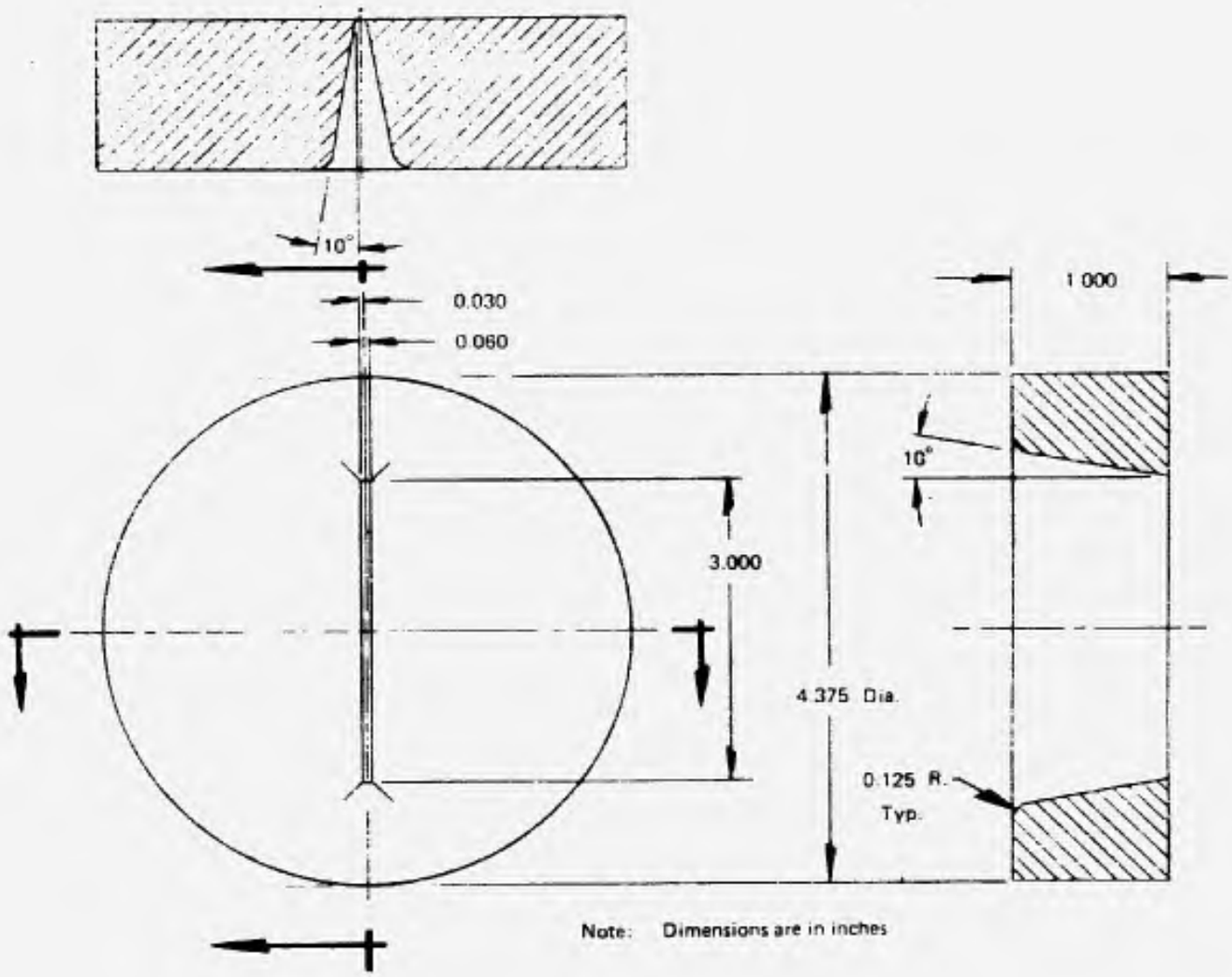

Figure 6. Rectangular Nozzle (Aspect Ratio, L/d = 50)

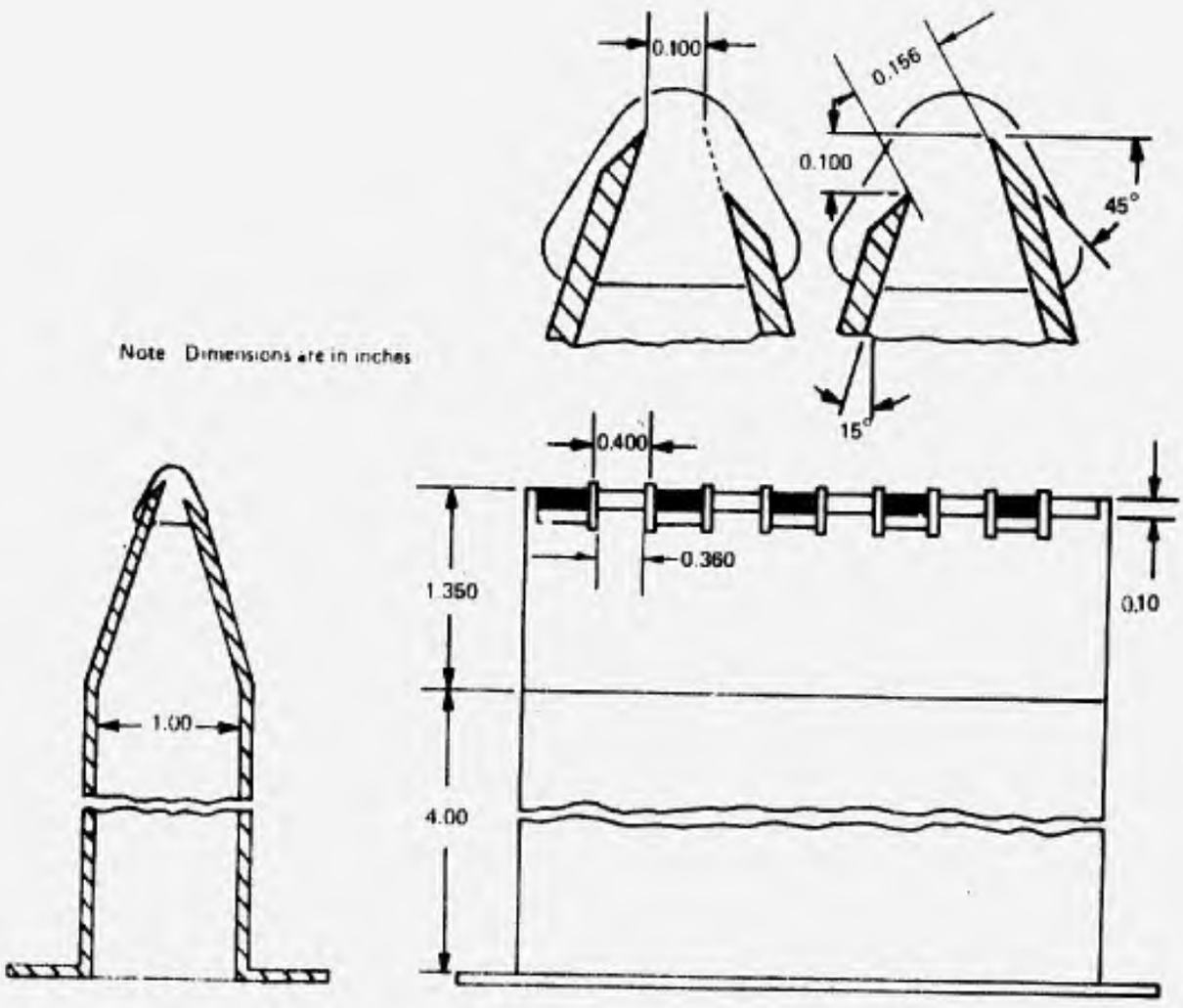

Figure 7. 0.4-Inch Alternating Exit Nozzle Detail

L/d	d,in.
AXI	0.480
1	0.425
10	0.1345
25	0.085
50	0.060

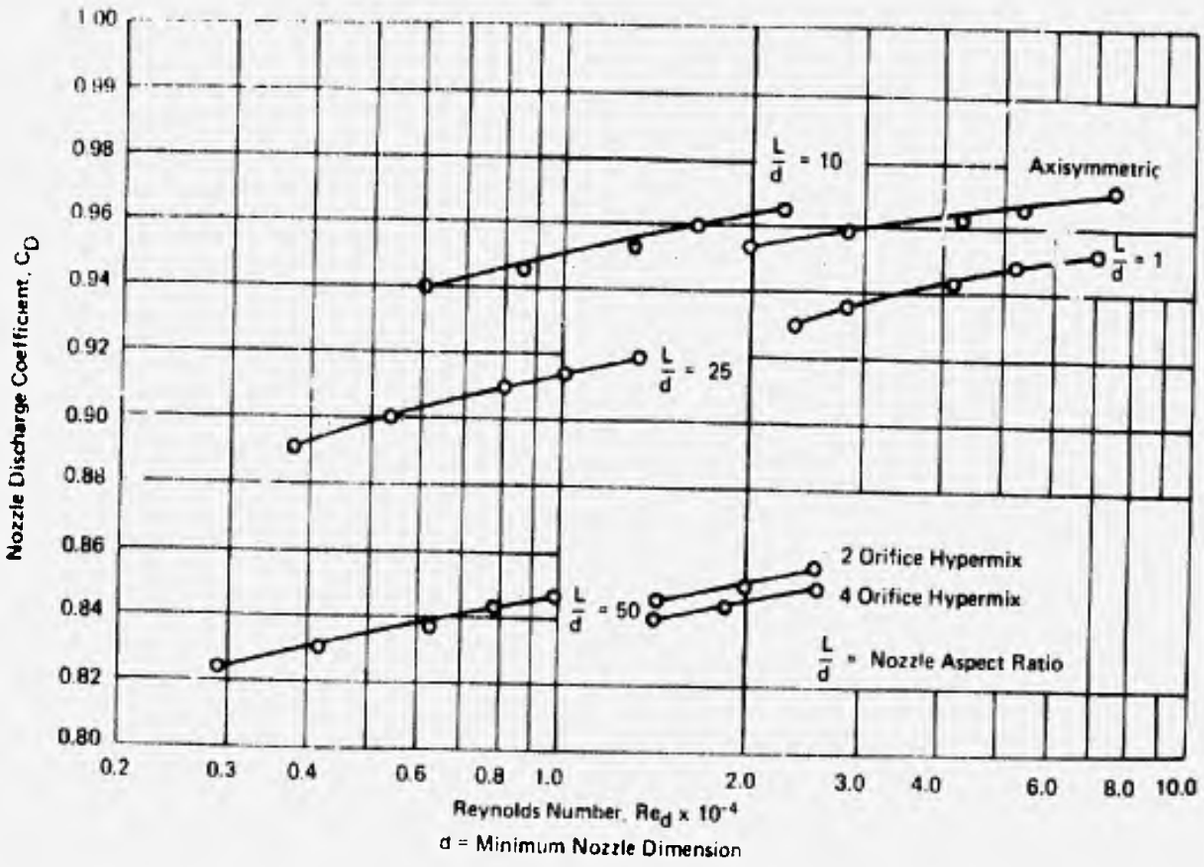

Figure 8. Nozzle Discharge Coefficients

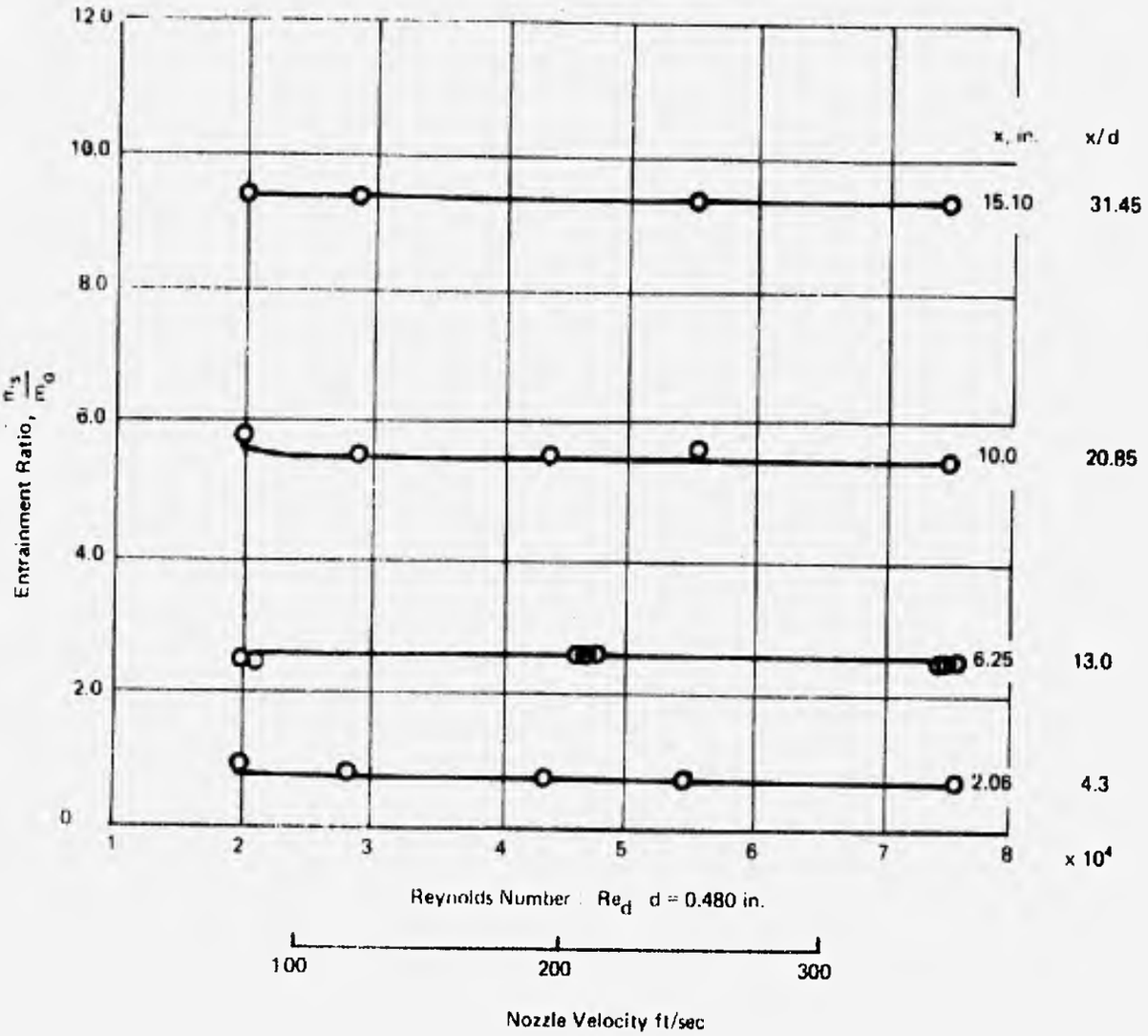

Figure 9. Entrainment Ratio as a Function of Reynolds Number Re_d - Axisymmetric Nozzle

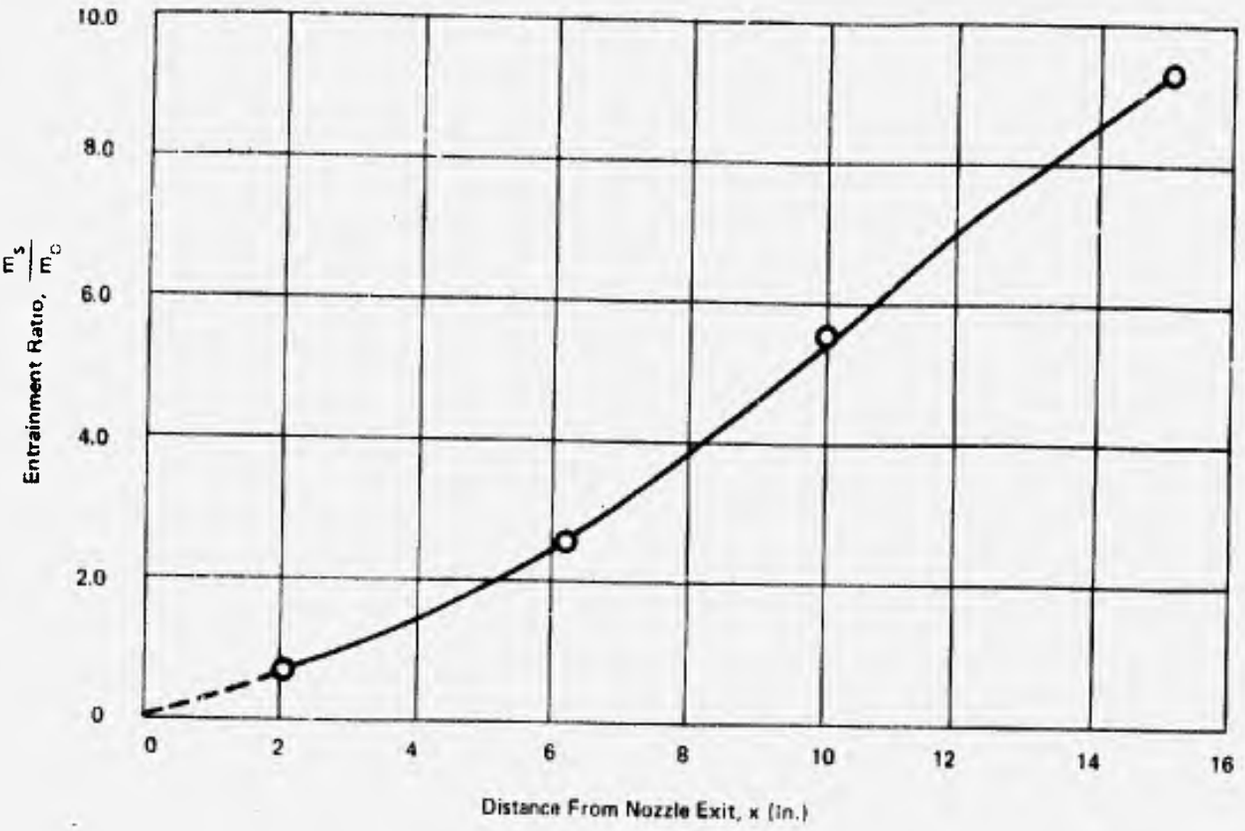

Figure 10. Entrainment Rate as a Function of Distance from Nozzle Exit Plane - Axisymmetric Nozzle

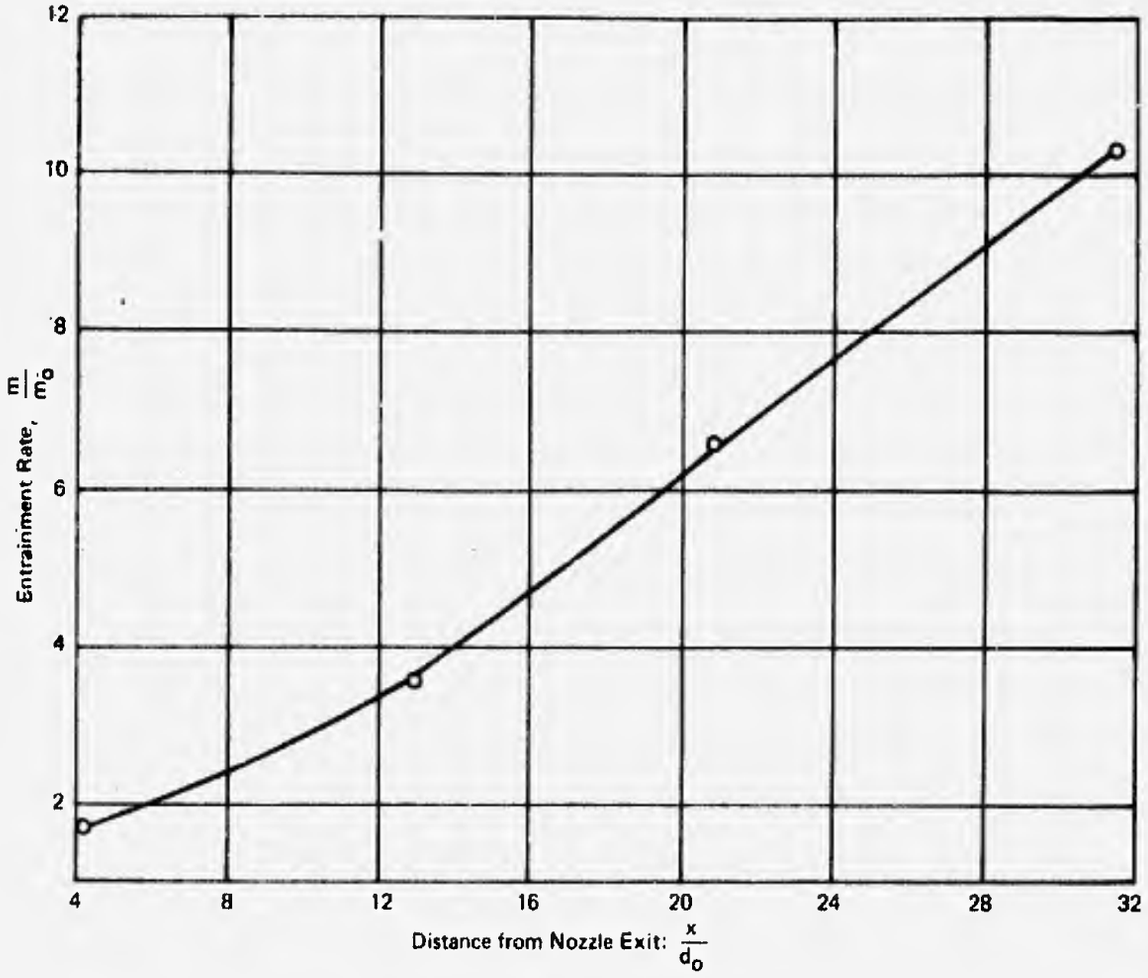

Figure 11. Entrainment Rate of Axisymmetric Jet

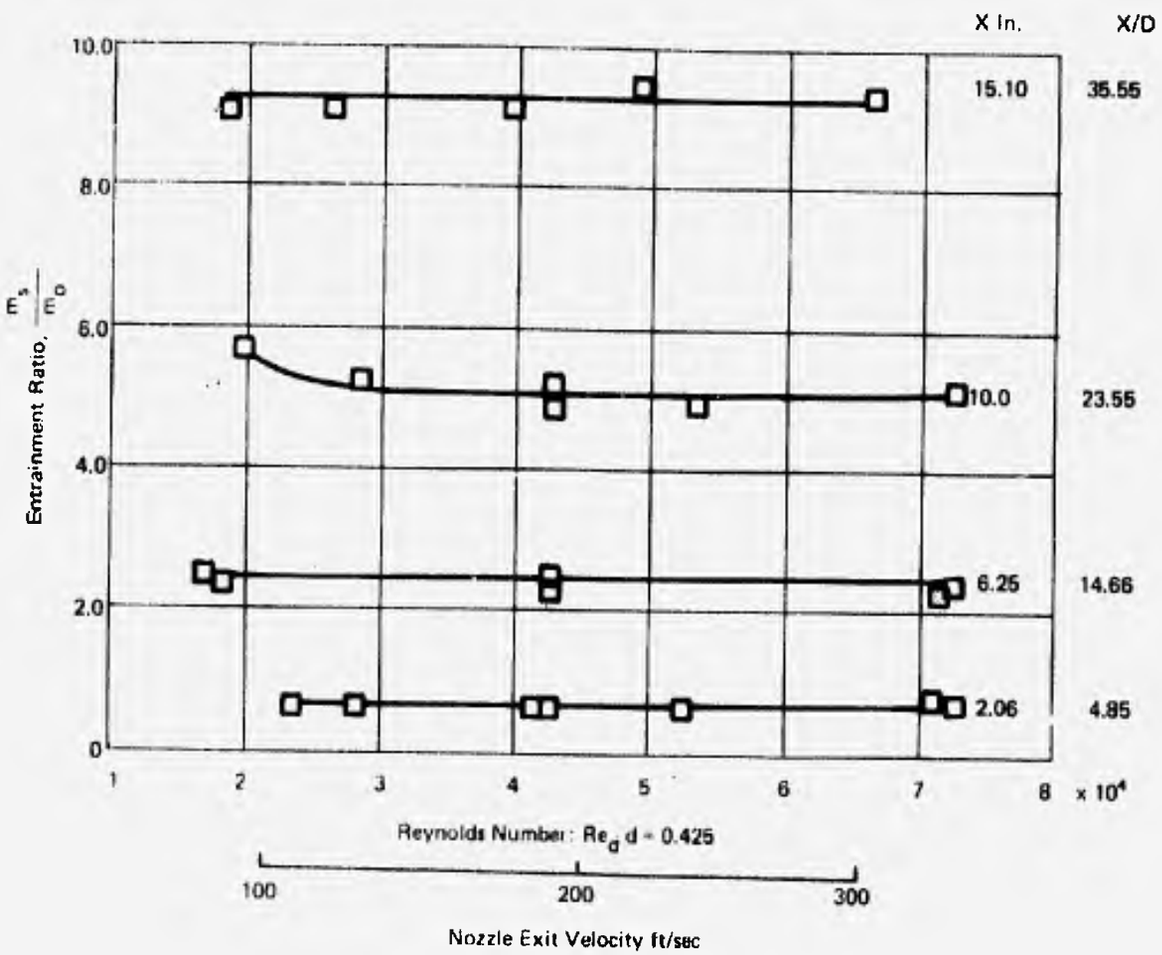

Figure 12. Entrainment Ratio as a Function of Reynolds Number Re_d - Square Nozzle

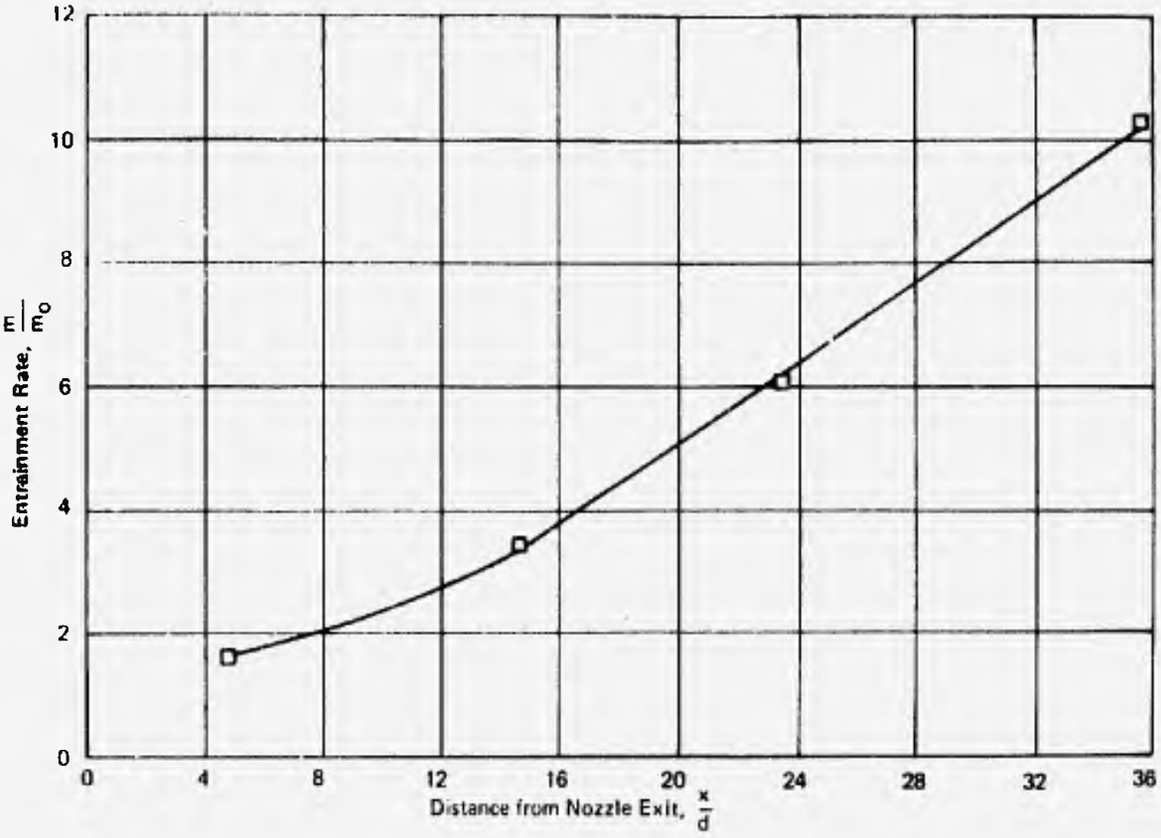

Figure 13. Entrainment Rate of Square Nozzle

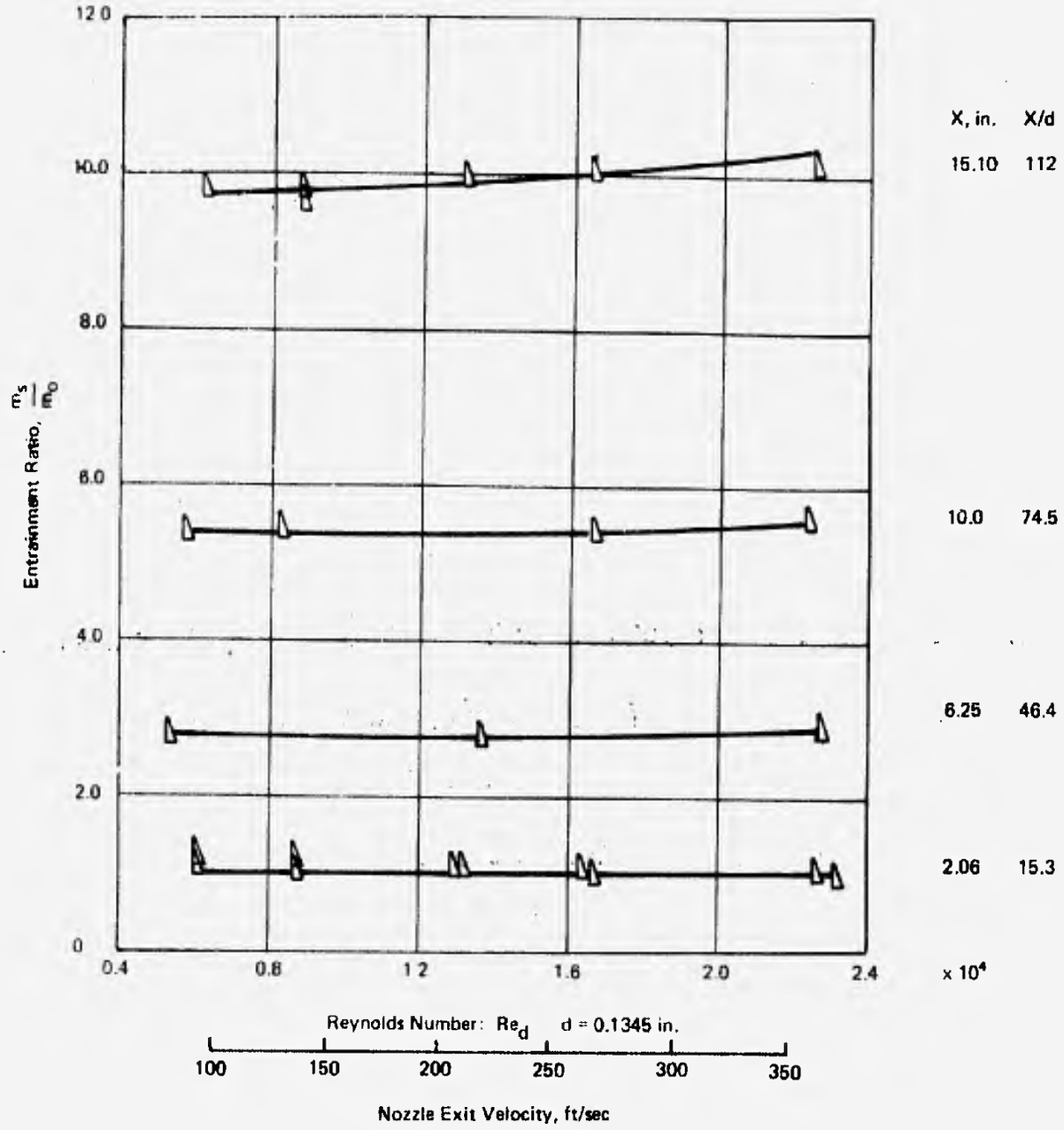

Figure 14. Entrainment Ratio as a Function of Reynolds No. Re_d - 10:1 Aspect Ratio Nozzle

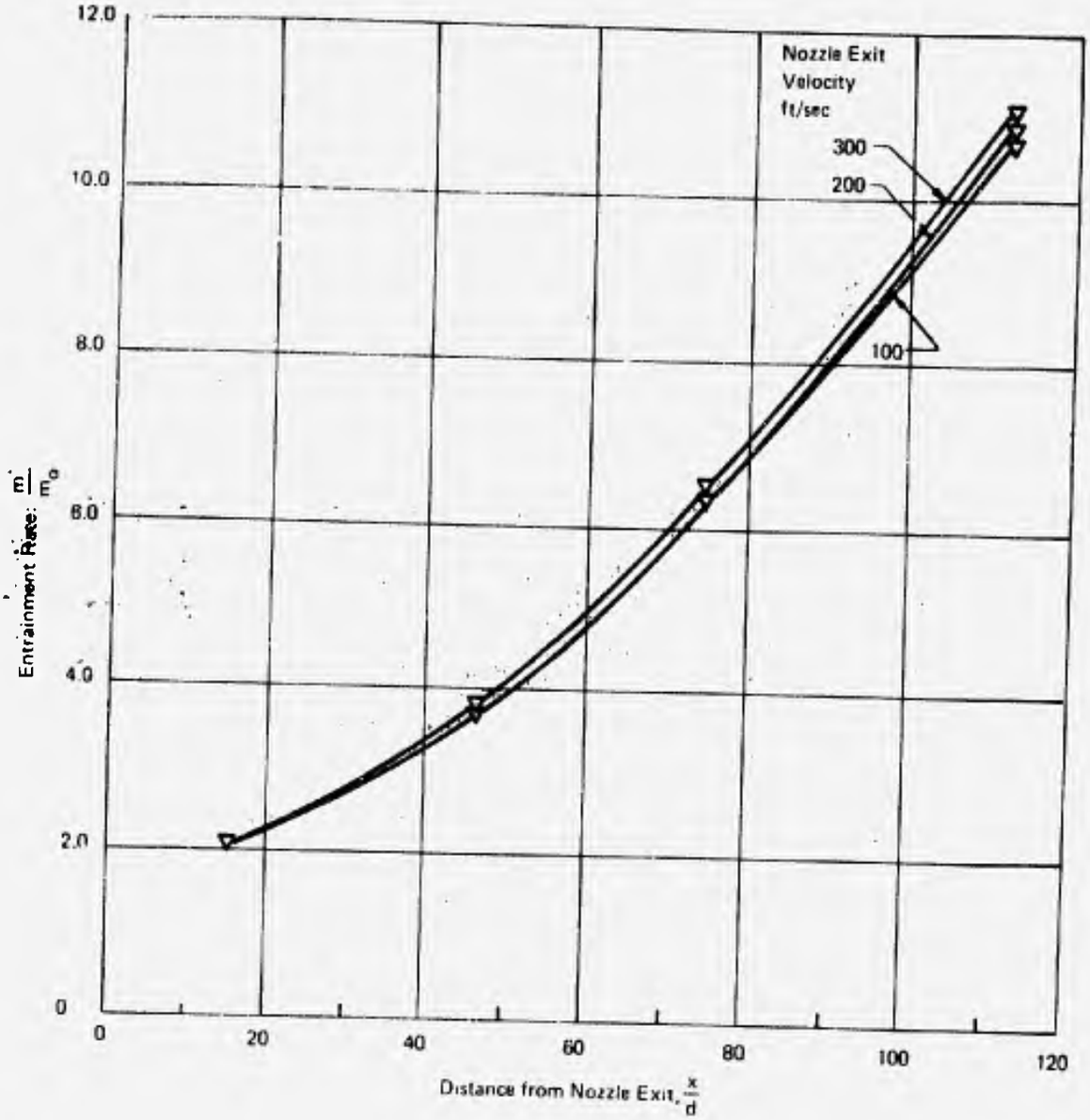

Figure 15. Entrainment Rate of 10:1 Aspect Ratio Nozzle

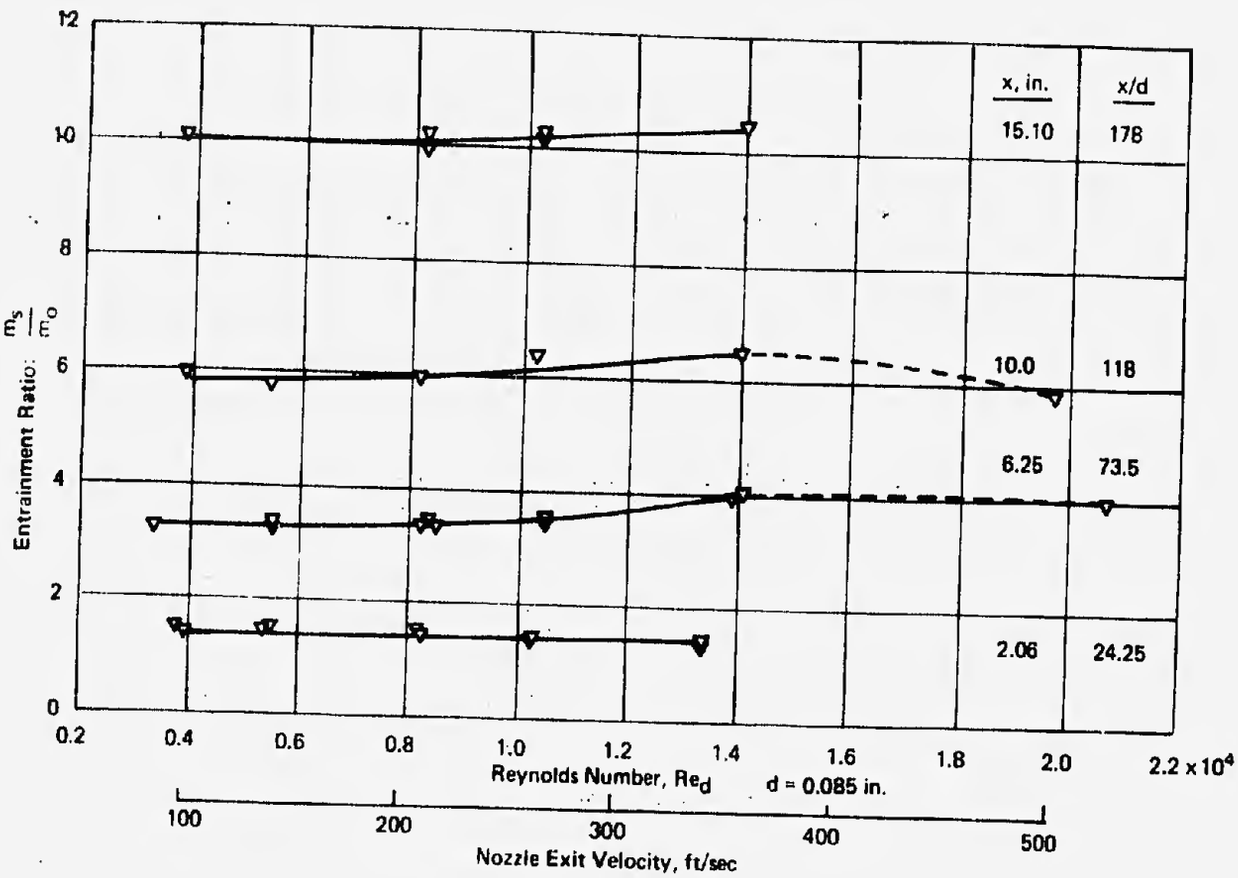

Figure 16. Entrainment Ratio as a Function of Reynolds No. Re_d - 25:1 Aspect Ratio Nozzle

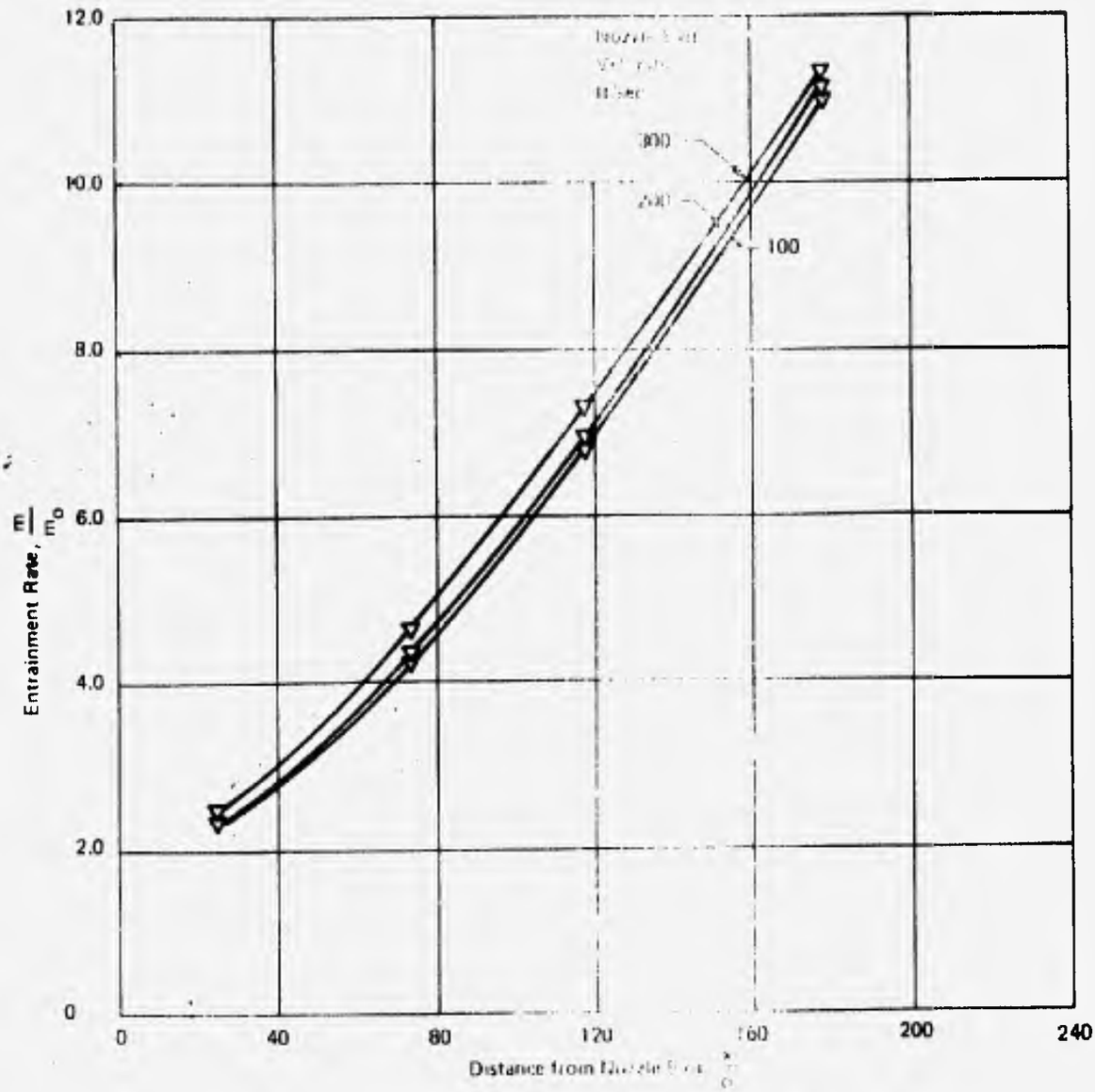

Figure 17. Entrainment Rate [illegible] Ratio Nozzle

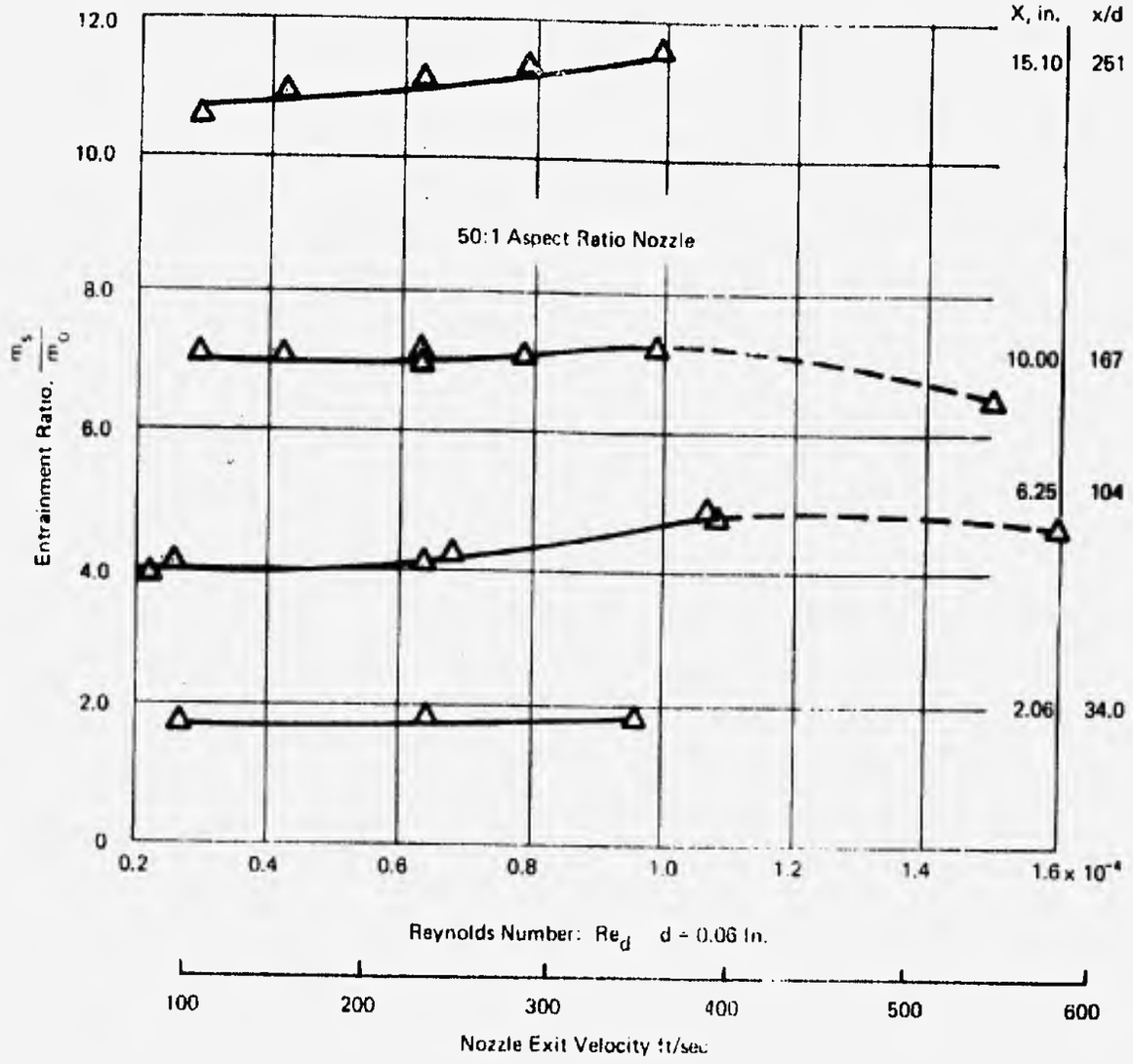

Figure 18. Entrainment Ratio as a Function of Reynolds No. Re_d - 50:1 Aspect Ratio Nozzle

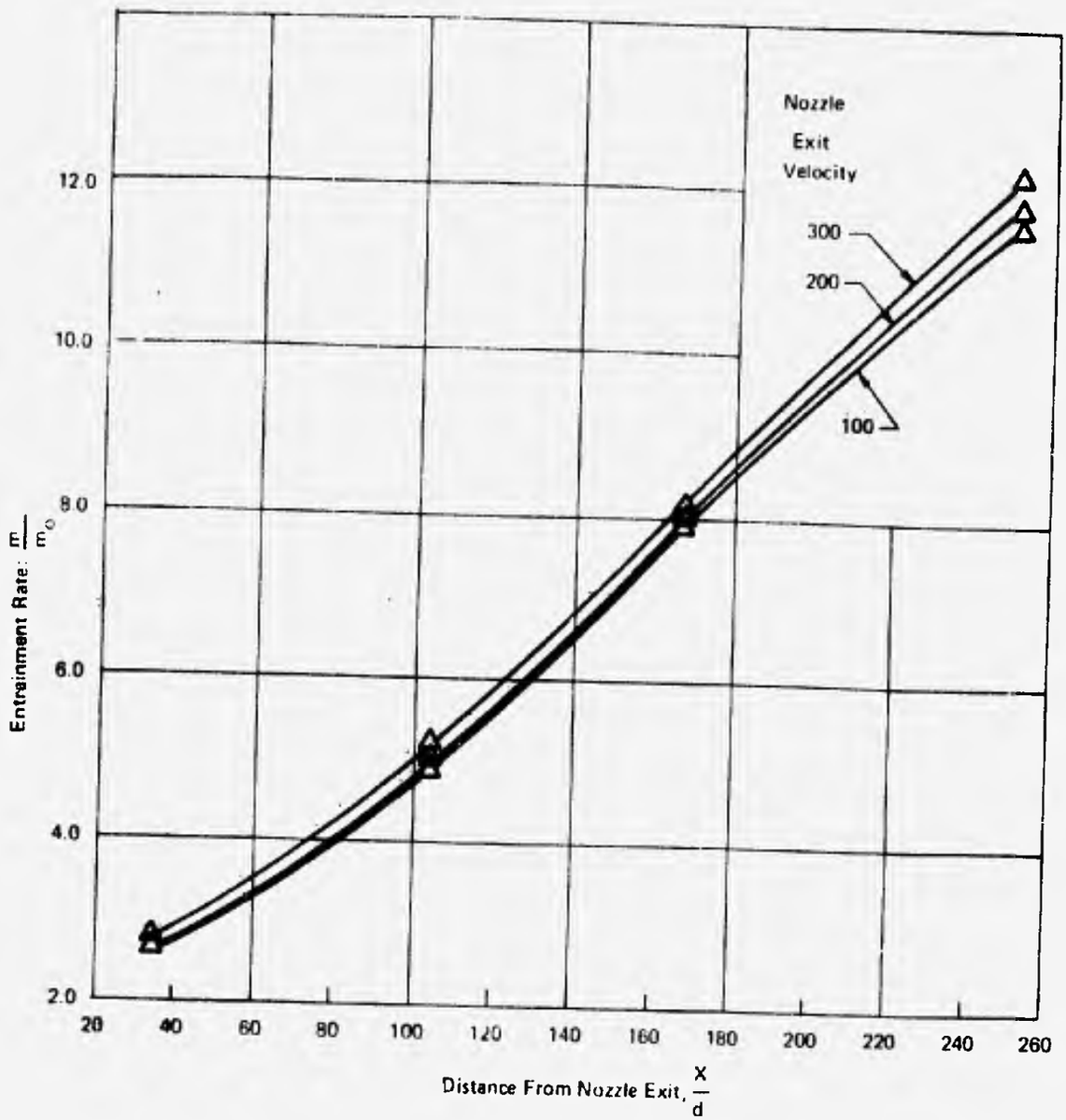

Figure 19. Entrainment Rate of 50:1 Aspect Ratio Nozzle

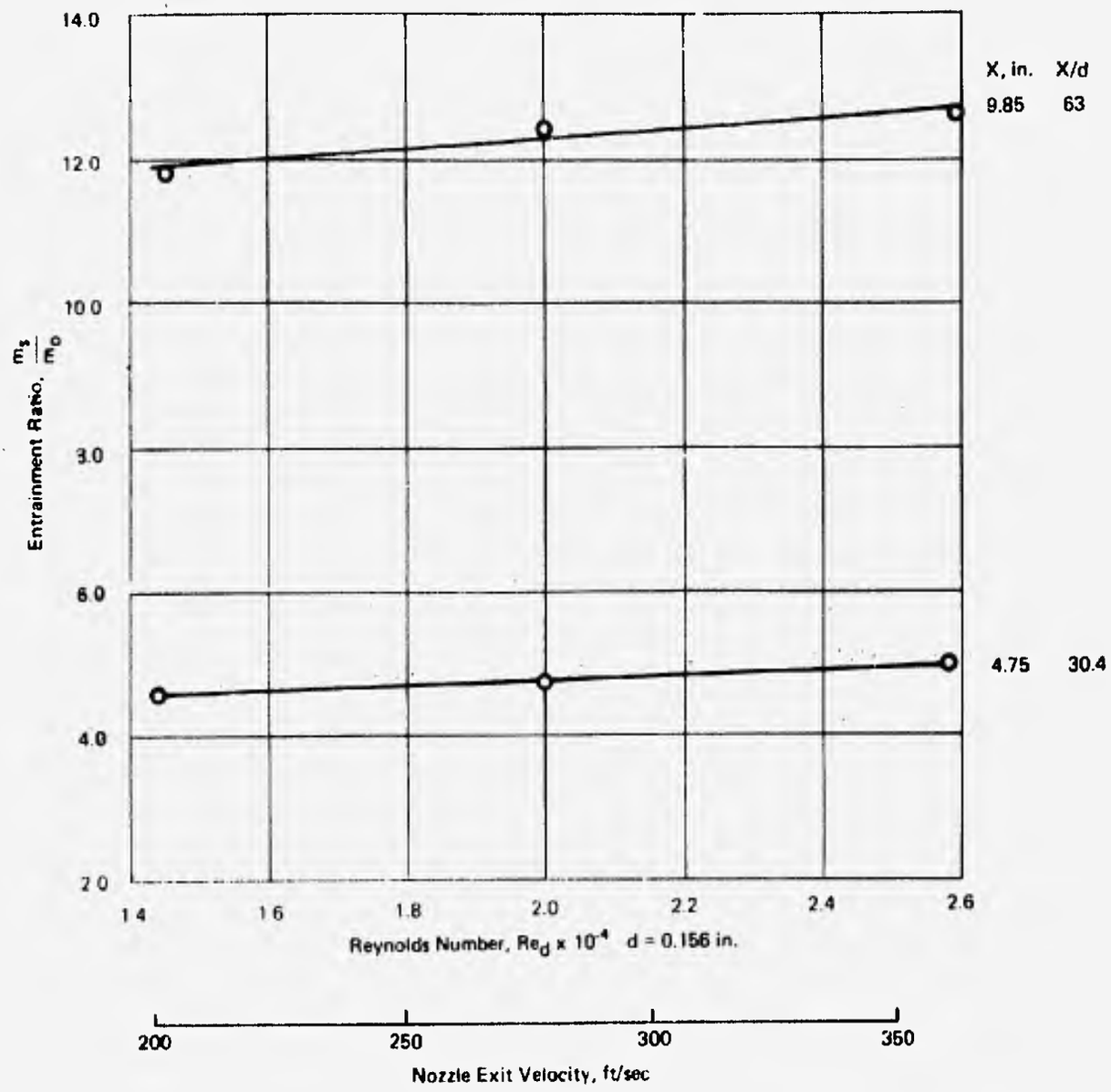

Figure 20. Entrainment Ratio as a Function of Reynolds No. Re_d-Two Orifice Hypermixing Nozzle

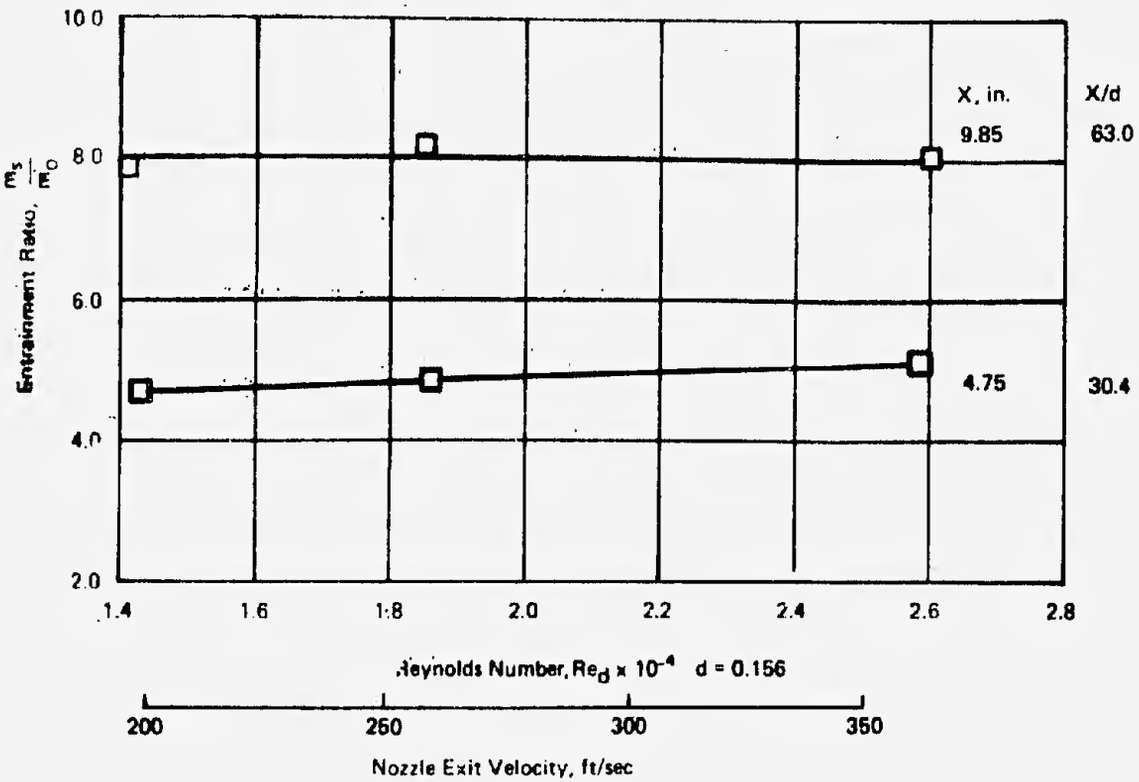

Figure 21. Entrainment Ratio as a Function of Reynolds No. Re_d - Four Orifice Hypermixing Nozzle

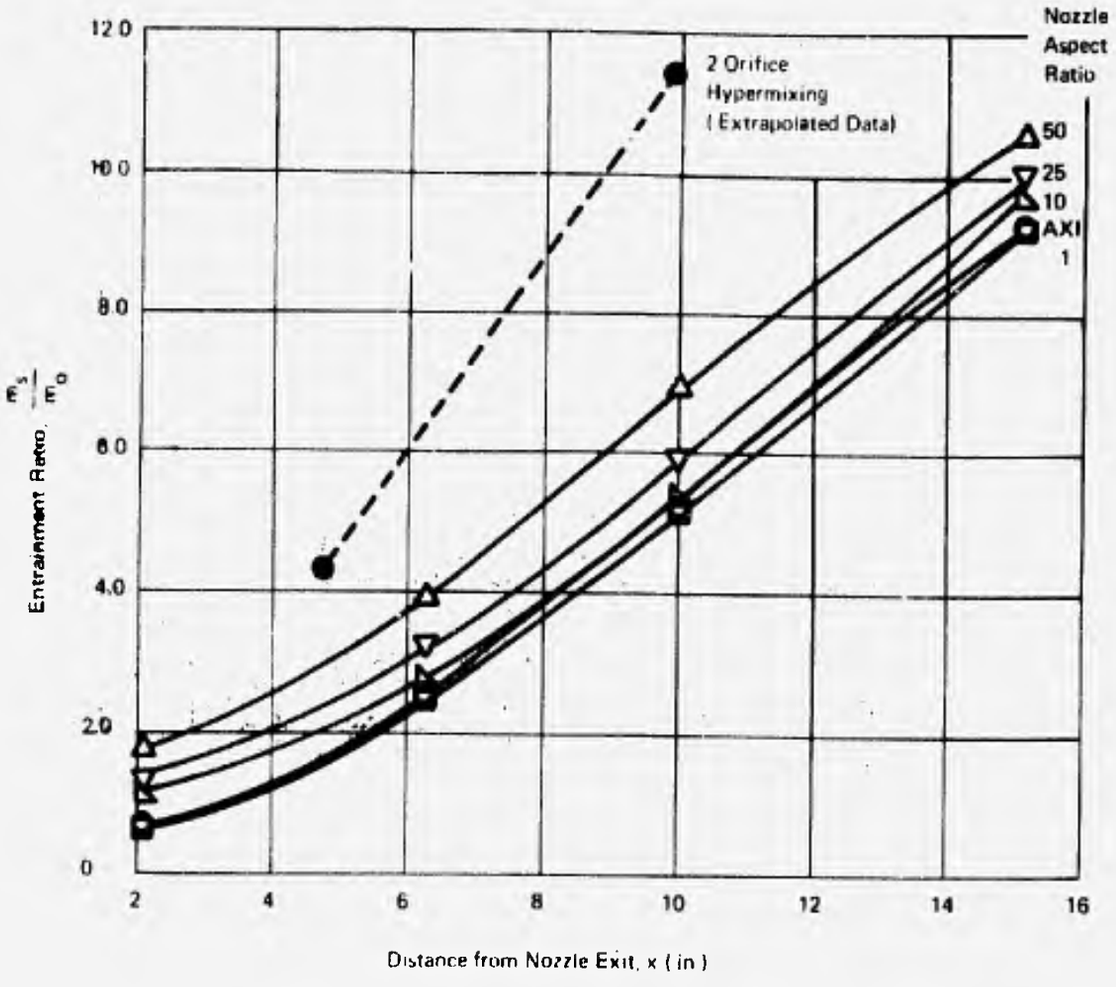

Figure 22. Entrainment Ratios of Nozzles U_{oc} = 100 ft/sec

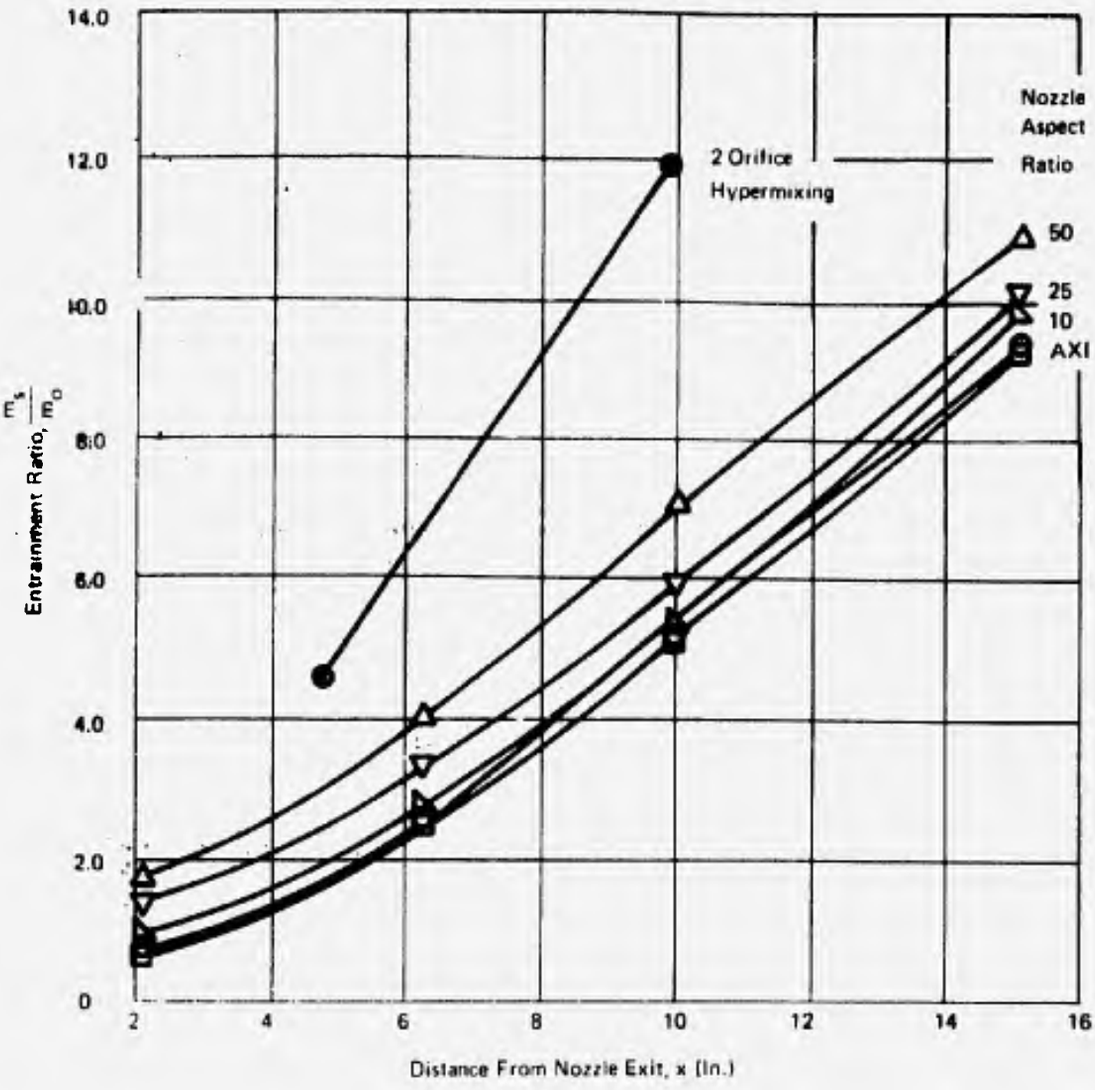

Figure 23. Entrainment Ratio of Nozzles U_{oc} = 200 ft/sec

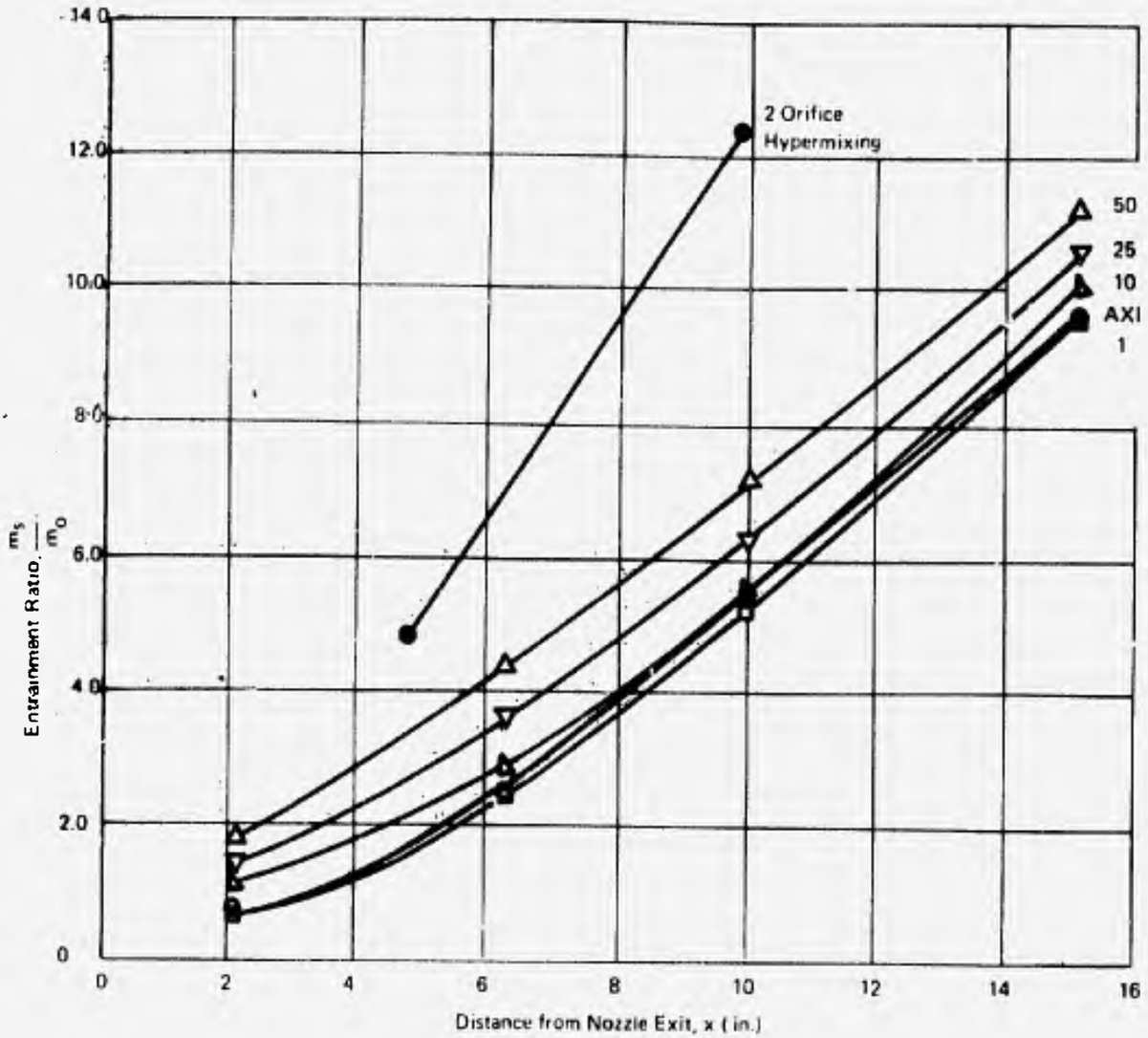

Figure 24. Entrainment Ratios of Nozzles U_{oc} = 300 ft/sec

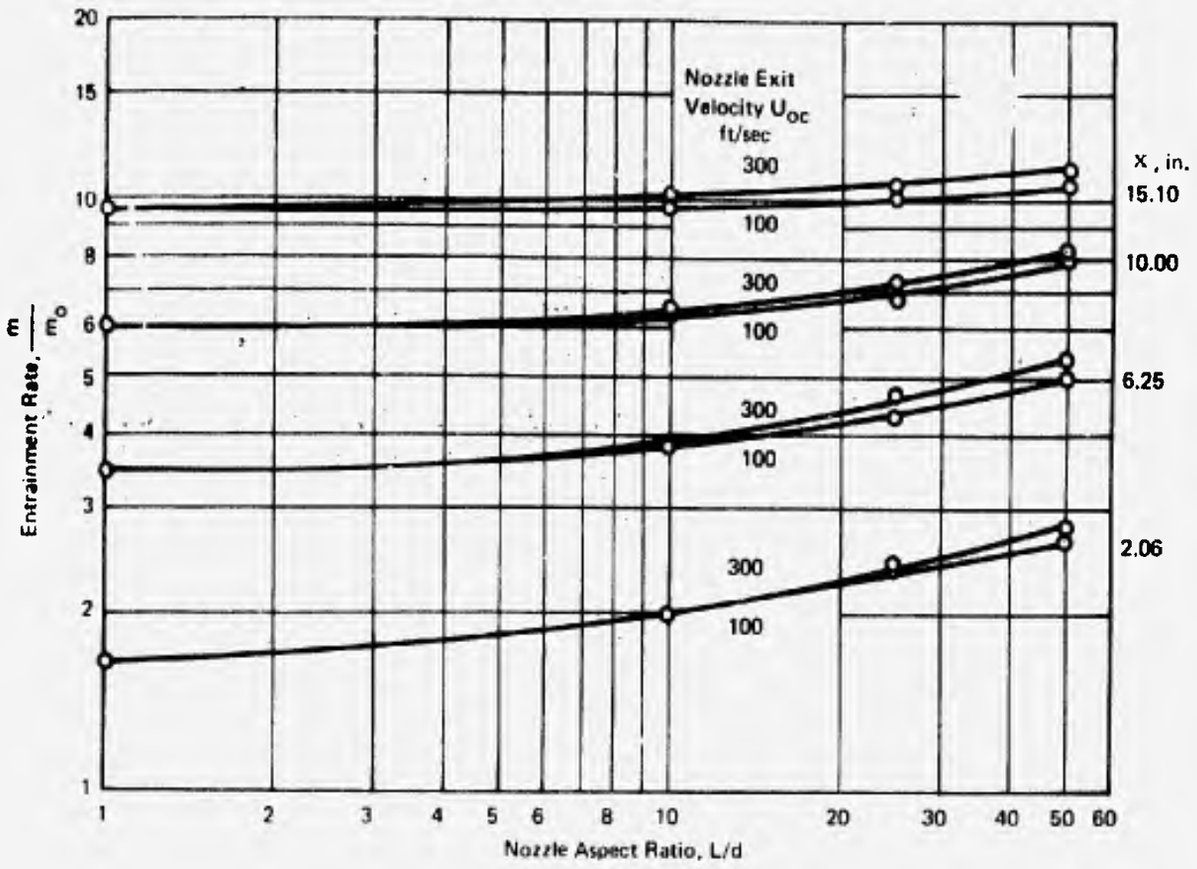

Figure 25. Entrainment Rate as a Function of Nozzle Aspect Ratio

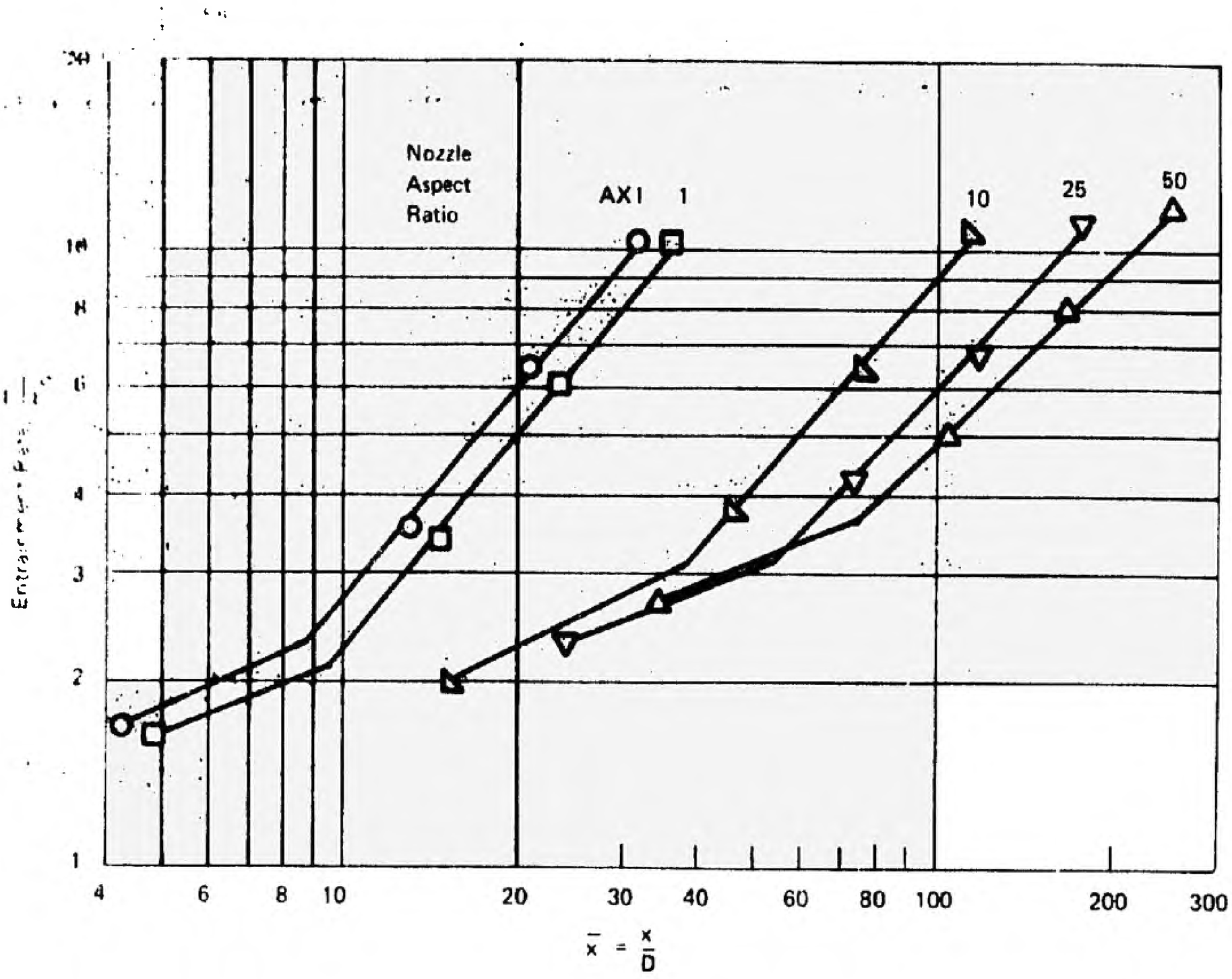

Figure 26. Entrainment Rates of Nozzles as a Function of $\bar{x}$, U_{oc} = 100 ft/sec

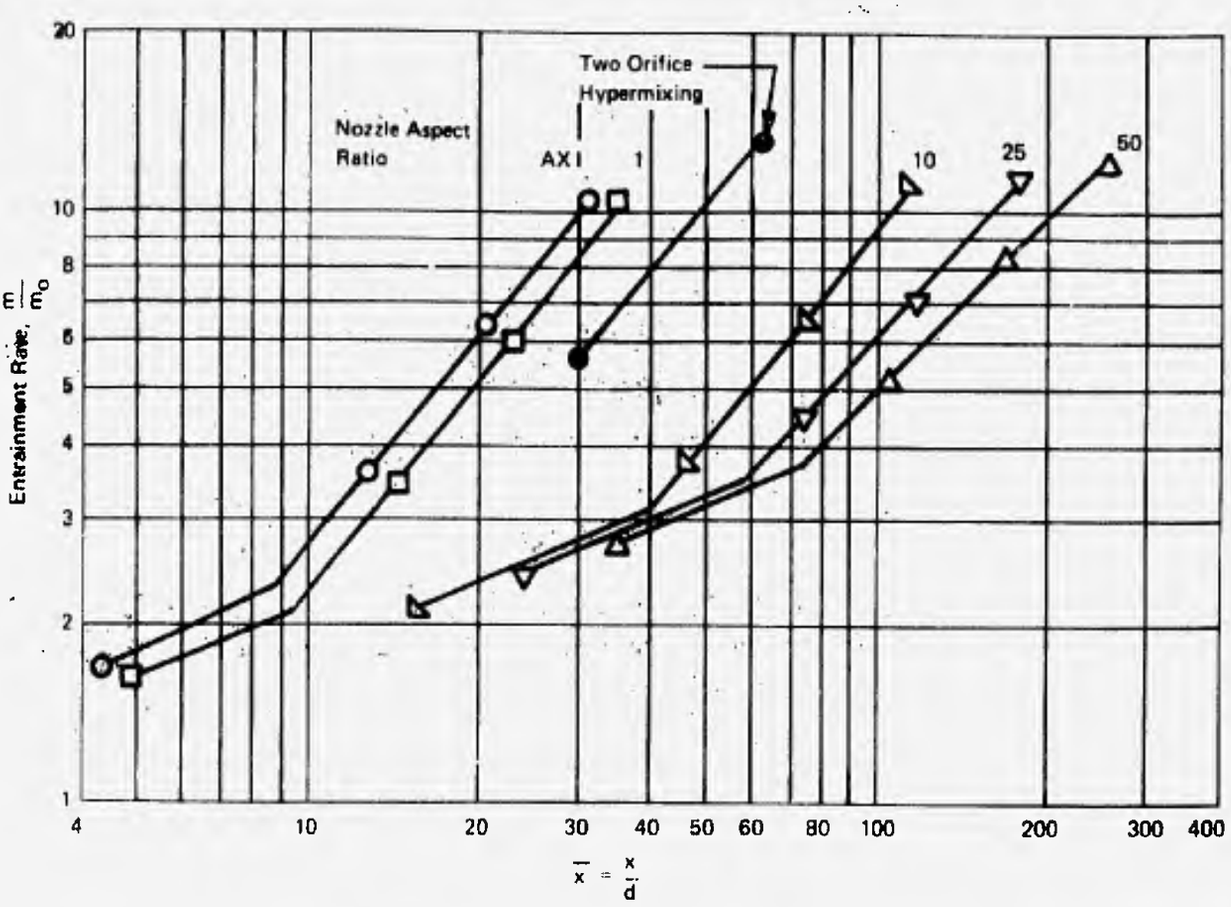

Figure 27. Entrainment Rates of Nozzles as a Function of $\bar{x}$, U_{oc} = 200 ft/sec

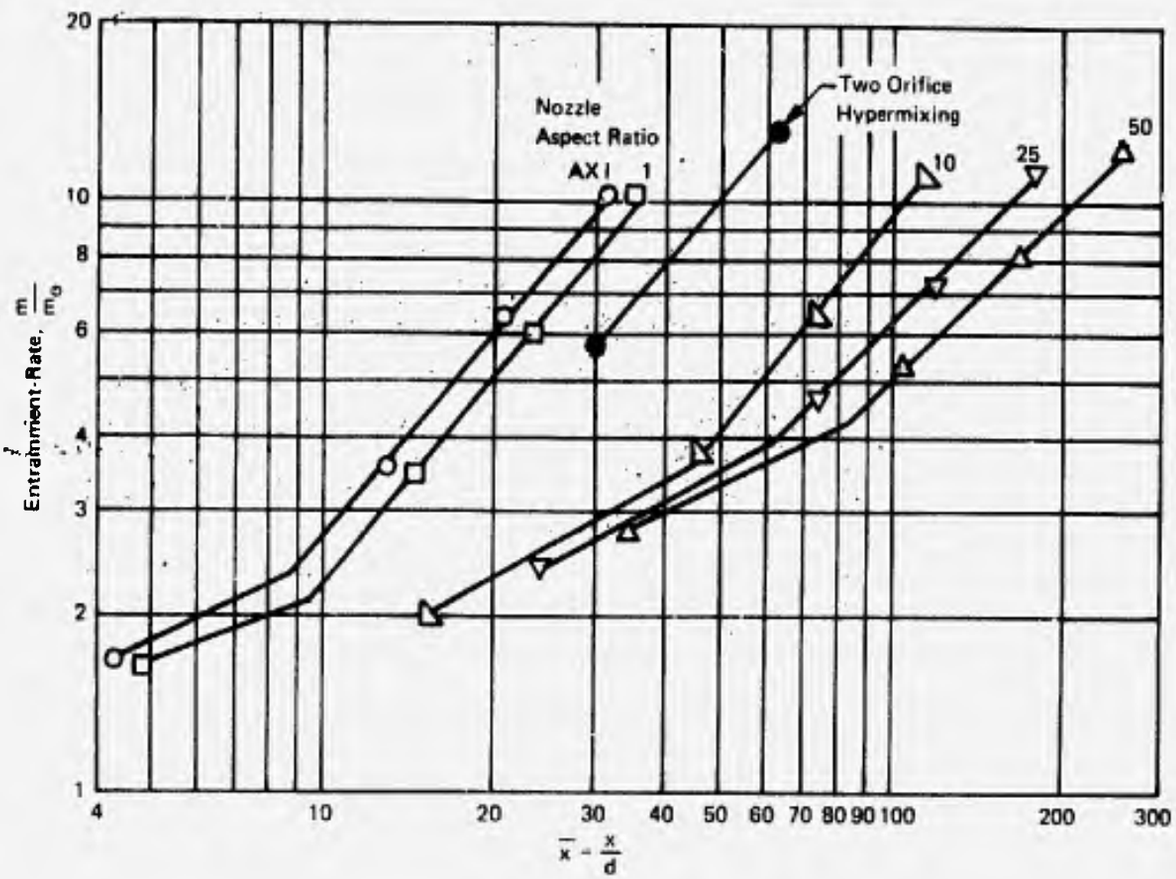

Figure 28. Entrainment Rates of Nozzles as a Function of $\bar{x}$, U_{oc} = 300 ft/sec

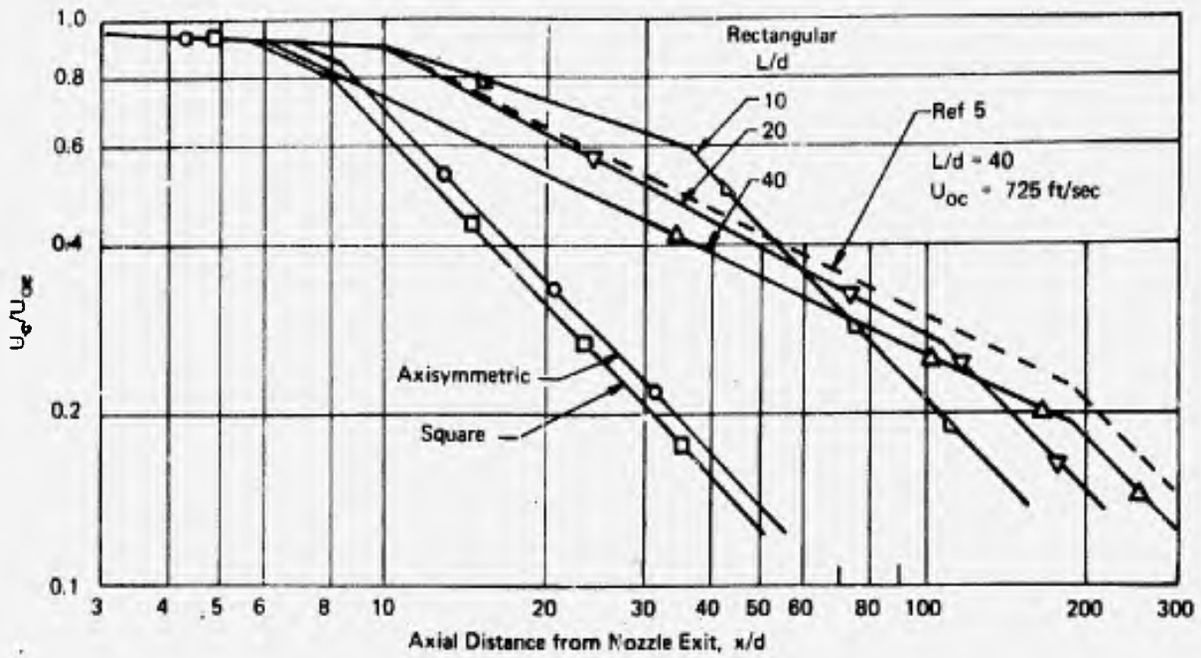

Figure 29. Axis Velocity Decay of Various Nozzles (Ref. 7) (Points Shown Are Values of x/d Where Entrainment Data Were Obtained)

APPENDIX A
PRELIMINARY EXIT APERTURE TESTS

Data for velocity half-width variation as a function of distance from the primary nozzle exit are present in the literature (Reference 1). These data do not, however, indicate their degree of applicability to rectangular nozzle flows when the primary jet velocity is varied. Some of the scatter in preliminary data obtained at the highest velocity of interest could be attributed to interference with the flow by the orifice plate. The exit aperture angle (defined as the angle at the apex of the cone formed between the exit aperture diameter and the nozzle exit diameter) for these tests was 32 degrees. This selection was based on the results of Ricou and Spalding (Reference 3) and Hill (Reference 8).

Several additional aperture plates were tested with both the axisymmetric and rectangular nozzles at an entrainment chamber length, x = 6.25 inches. Isentropic nozzle exit velocities up to 340 ft/sec were used to ensure adequacy of the measurements over the entire velocity range.

Figures A-1 through A-4 show the results of preliminary tests which guided the selection of apertures for the entire test program. The ordinate is the exit aperture pressure differential (excess pressure in the chamber measured with respect to atmospheric pressure) while the abscissa is the entrainment ratio (ratio of air flow rate through the porous wall, m_s to the primary air flow rate, m_o) for a fixed primary flow rate. Each curve shown in a figure is for a different exit aperture angle. Data are presented for the axisymmetric nozzle and the rectangular nozzle with the greatest aspect ratio (L/d = 50).

The data show that the smallest aperture provides the greatest sensitivity of the pressure differential to variations in secondary flow. However, if the aperture angle is too small, an erroneously low value of the entrainment ratio (when the pressure differential is zero) is obtained. The data also show that the slope of the curve for a given aperture angle increases with increasing primary flow velocity. It is thus concluded that selection of an aperture diameter based on data acquired at the maximum primary jet velocity of interest is appropriate for testing at all lesser velocities. This assumes, of course, that adequate changes in pressure differential are obtained at the minimum primary jet velocities tested.

At the minimum distance, X = 2.06 inches, from the single nozzle exit plane, the selection of aperture diameter was governed by the maximum dimension, L of the nozzle exit.

On the basic of the above considerations, the aperture diameters used in the investigation are tabulated in Table A-1.

TABLE A-I
EXIT APERTURE DIAMETERS USED FOR
MASS ENTRAINMENT MEASUREMENT

$X^{(1)}$ (in.)	Exit Aperture Diameter (in.)					
	Primary Nozzle					
	AXI	1:1	10:1	25:1	50:1	HYPER
2.06	1.94 2.50	2.50	3.391 3.794	3.391 3.794	3.794 4.060	
6.25	4.06 5.04 5.50 5.66	5.04 5.66	5.66	5.04 5.66	5.04 5.50 5.66 6.687	
10.00	8.33	8.33	8.33 9.38	8.33 9.38	8.33 9.38	
15.10	12.90	12.90	12.90	12.90	11.39 12.90	
4.75						9.38 11.38 12.90
9.85						11.38 12.90

(1) Distance from Nozzle Exit Plane to Exit Aperture

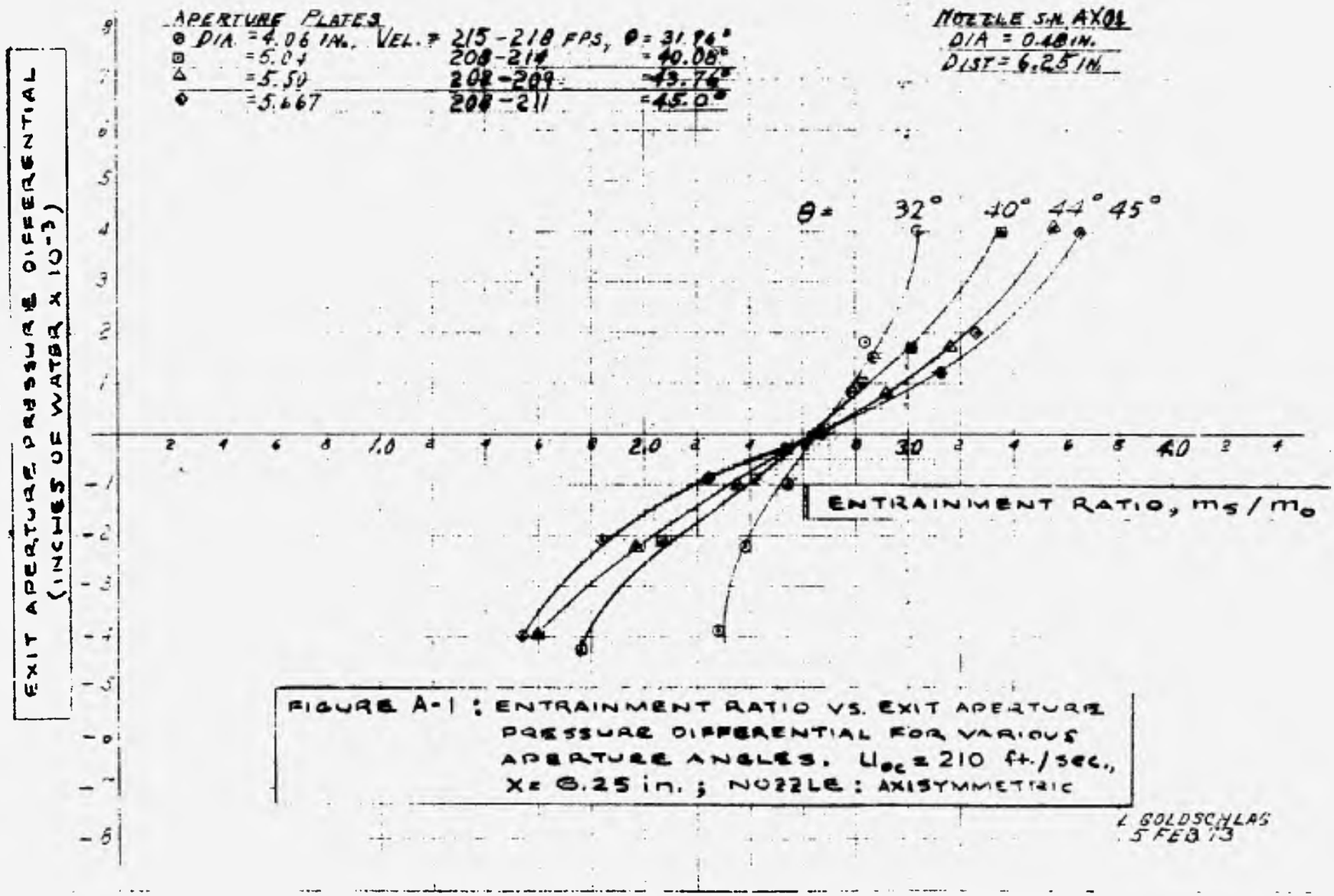

FIGURE A-1 : ENTRAINMENT RATIO VS. EXIT APERTURE PRESSURE DIFFERENTIAL FOR VARIOUS APERTURE ANGLES. U_{oc} = 210 ft./sec., X = 6.25 in. ; NOZZLE : AXISYMMETRIC

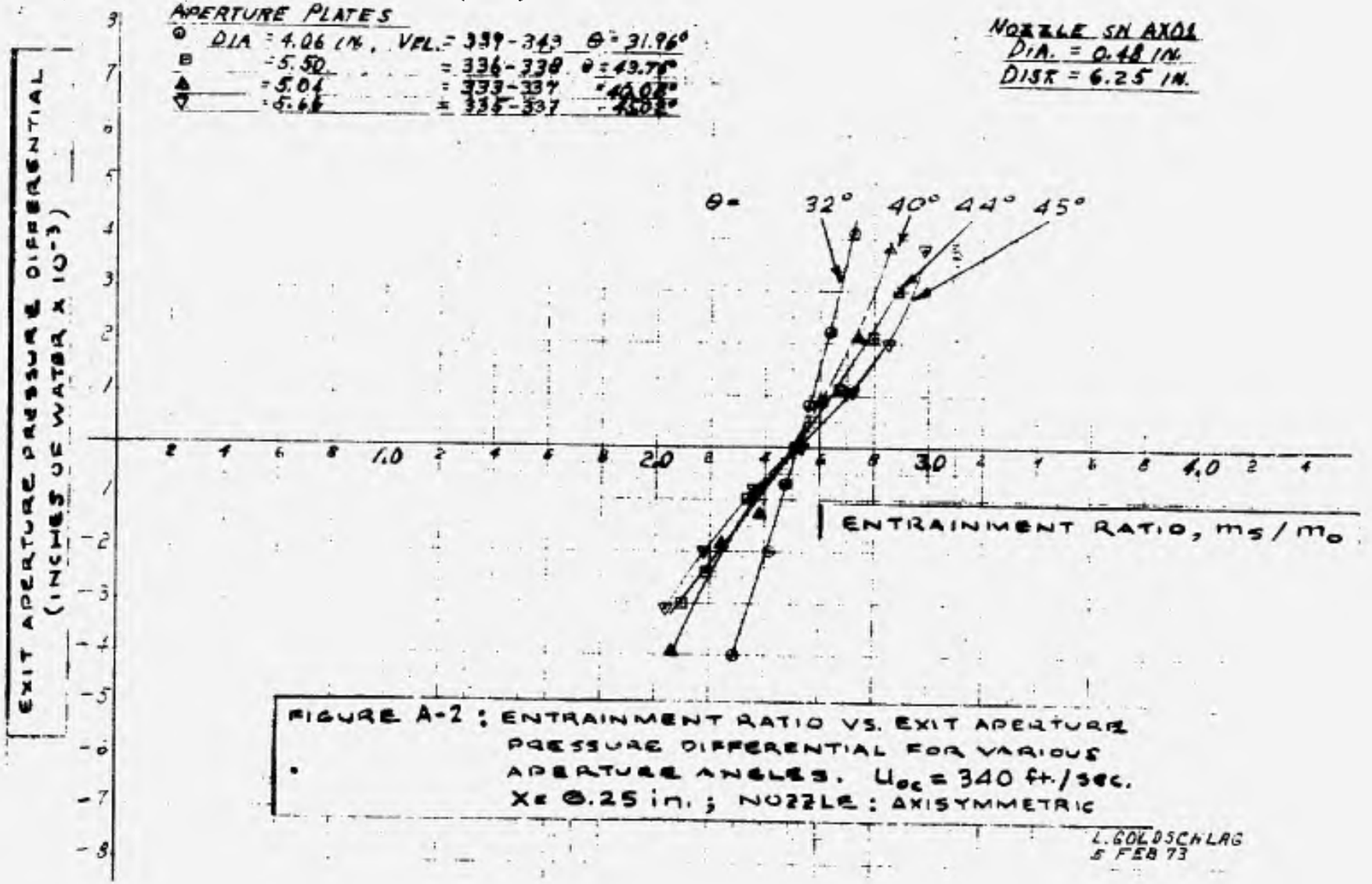

FIGURE A-2 : ENTRAINMENT RATIO VS. EXIT APERTURE PRESSURE DIFFERENTIAL FOR VARIOUS APERTURE ANGLES. U_{oc} = 340 ft./sec. X = 0.25 in.; NOZZLE : AXISYMMETRIC

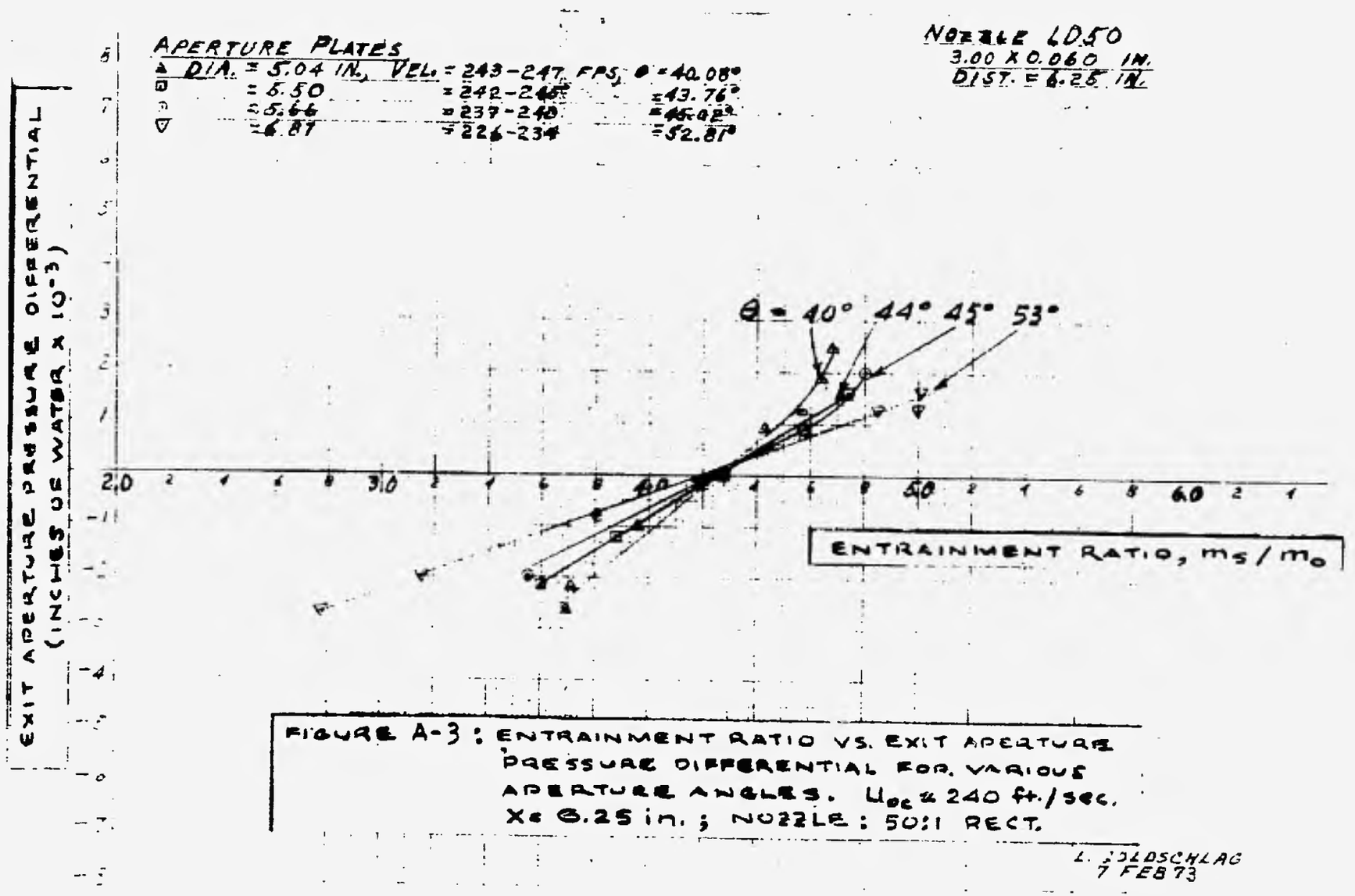

FIGURE A-3 : ENTRAINMENT RATIO VS. EXIT APERTURE PRESSURE DIFFERENTIAL FOR VARIOUS APERTURE ANGLES. $U_{oc} \approx 240$ ft./sec. X = 6.25 in. ; NOZZLE : 50:1 RECT.

L. GOLDSCHLAG
7 FEB 73

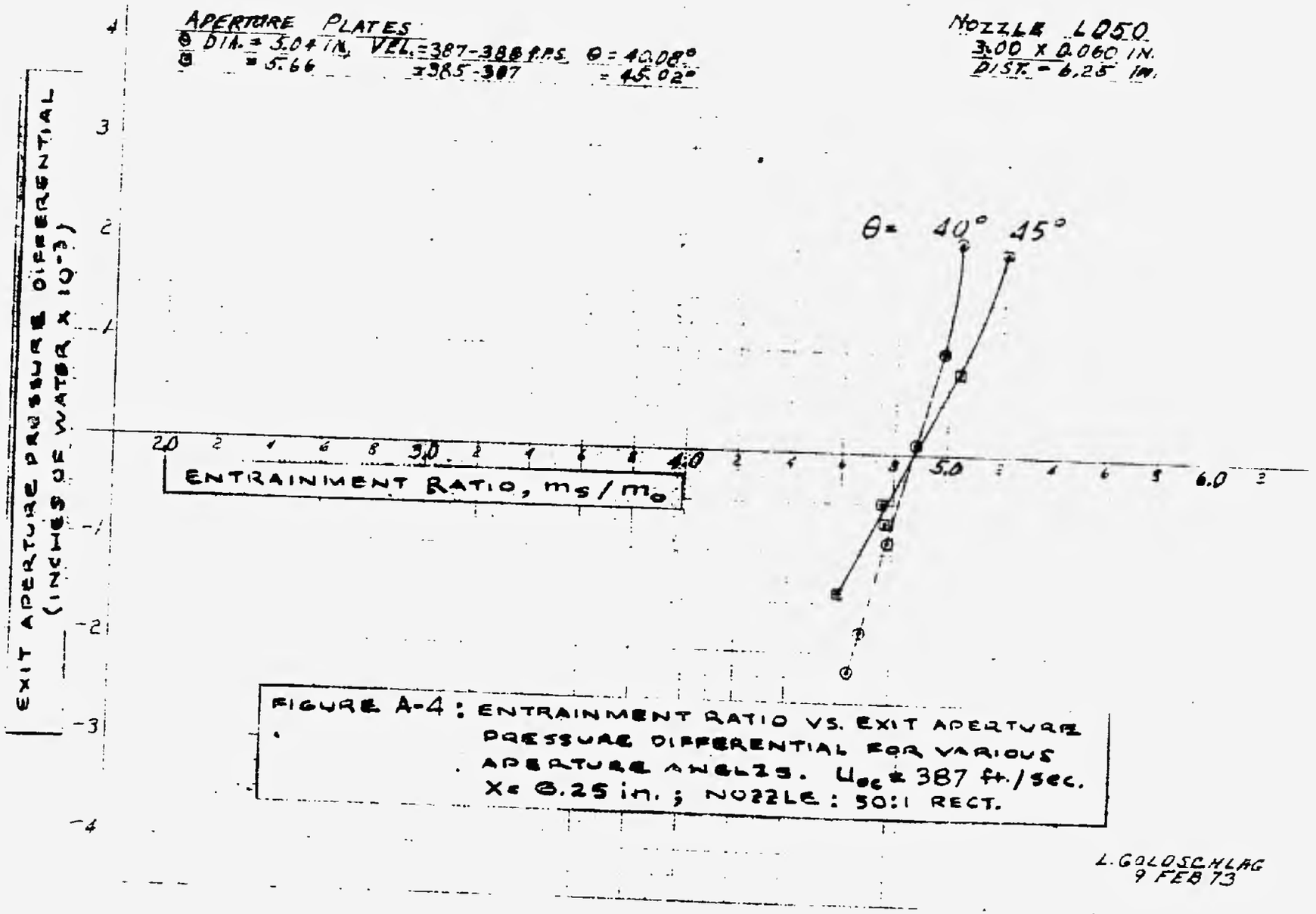

FIGURE A-4 : ENTRAINMENT RATIO VS. EXIT APERTURE PRESSURE DIFFERENTIAL FOR VARIOUS APERTURE ANGLES. U_{oc} = 387 ft./sec. X = 6.25 in. ; NOZZLE : 50:1 RECT.

L. GOLOSCHLAG
9 FEB 73

APPENDIX B
COMPUTER CODING

An average of three test runs for each primary jet velocity, each at a different secondary weight flow rate, were required for each data point. To facilitate the reduction of the large amount of test data, a computer program was written.

The nomenclature and computer coding are presented in Table B-1 and Figure B-1, respectively. An example of the computer Input/Output is presented in Figure B-2.

TABLE B-I
NOMENCLATURE
COMPUTER CODING

INPUT CODING

ROTO	Flowmeter reading, percent of full scale.
P41 (PSIG)	Primary flowmeter gas pressure, psig.
T7 (MV)	Primary flowmeter gas temperature and stagnation temperature, mv.
P42 (PSIG)	Secondary flowmeter gas pressure, psig.
T8 (MV)	Secondary flowmeter gas temperature, mv.
PO (PSIG)	Nozzle plenum (stagnation) pressure, psig.
PPL PO	Nozzle Pressure Ratio.
PAP (MV)	Exit aperture pressure differential, mv.
Z(1), Z(2), Z	Exit aperture pressure transducer null points, mv.
CON	Secondary flowmeter range factor.

OUTPUT CODING

ROTO	Flowmeter reading, percent of full scale.
P (PSIA)	Primary flowmeter gas pressure psia.
T(R)	Primary flowmeter gas temperature, °R.
Q (SCFM)	Primary volumetric flow rate scfm.
MP (MLB/S)	Primary weight flow rate, $\frac{lb}{sec} \times 10^{-3}$.
VP (FT/SEC)	Isentropic nozzle exit velocity, ft/sec.
RE	Nozzle Reynolds number based on d = 0.480 in.
C_D	Nozzle discharge coefficient.
P (PSIA)	Secondary flowmeter gas pressure, psia.
T(R)	Secondary flowmeter gas temperature, °R.

TABLE B-1 (CONTD)

DPAP (MIW)	Exit aperture pressure differential, inches of water x 10^{-3}.
MS (MLB/S)	Secondary weight flow rate, lb/sec x 10^{-3}.
MS/MP	Ratio of secondary to primary weight flow rates.
MP + MS	Sum of secondary and primary weight flow rates.
TOT/MD	(MP + MS)/MP
TOT/MP/XD	(MP + MS)/MP ÷ x/d.
D = 0.48	Axisymmetric nozzle diameter, d, inches.
X	Length of entrainment chamber, inches.
DO	Exit aperture diameter, inches.
PBAR	Atmospheric pressure, psia.
THETA	Exit aperture angle referred to axisymmetric nozzle.
MS/MP INT	Two-point intercept for DPAP = 0.

```
/display extract
L.0073  ACTION IS PROCESS
L.0001  /JOB GO
L.0002  /FTC
L.0003        DIMENSION BX1(35),BX2(35),BX3(35),BX4(35),BX5(35),BX6(35),BX7(35),
L.0004       *BX8(35),BX9(35),BX10(35),BX11(35),BX12(35),BX13(35)
L.0005        DIMENSION BX14(35),BX15(35),BX16(35)
L.0006        DIMENSION HEAD(18)
L.0007     23 CONTINUE
L.0008        WRITE(6,8)
L.0009      8 FORMAT(1H1)
L.0010     10 CONTINUE
L.0011        READ(5,9) (HEAD(I),I=1,18)
L.0012        WRITE(6,9) (HEAD(I),I=1,18)
L.0013      9 FORMAT(18A4)
L.0014        READ(5,7) DIA,X,PBARIN,DO
L.0015      7 FORMAT(8F10.5)
L.0016        WRITE(6,10)
L.0017     10 FORMAT(18X,'XD',16X,'PBAR',18X,'AP')
L.0018        PBAR = PBARIN * 0.001576
L.0019        XL = DIA/12.
L.0020        XD = X/DIA
L.0021        AP = 0.18096
L.0022        R = DO/2.
L.0023        RADTAN = ATAN((R-(DIA/2.))/X)
L.0024        THETA = RADTAN * (180./3.1416)
L.0025        THETA = THETA * 2.
L.0026        WRITE(6,11) XD,PBAR,AP
L.0027     11 FORMAT(5E20.5,///)
L.0028        WRITE(6,13)
L.0029     13 FORMAT(25X,'PRIMARY',51X,'SECONDARY'/)
L.0030        WRITE(6,14)
L.0031     14 FORMAT(1X,56('-'),2X,61('-'),//)
L.0032        WRITE(6,15)
L.0033        WRITE(6,16)
L.0034     15 FORMAT(2X,'ROTO',5X,'P',5X,'T',5X,'Q',5X,'HP',
L.0035       *5X,'VP',9X,'PF',5X,'CD',
L.0036       *4X,'ROTO',5X,'P',5X,'T',2X,'DPAP',5X,'HS',
L.0037       *4X,'HS/HP',1X,'HP+HS',1X,'POT/HP',1X,'POT/HP/VP')
L.0038     16 FORMAT(4X,'(F)',1X,'(PSIA)',3X,'(R)',
L.0039       *'(SCFM)',2X,'HP/S',
L.0040       *1X,'FT/SEC',
```

Figure B-1. Data Reduction Coding

Reproduced from best available copy.

```
L.0041        *21X,'(F)',1X,'(PSIA)',3X'(R)','( MTU)',
L.0042        *2X,'MM/S',
L.0043        *3X)
L.0044       22 CONTINUE
L.0045       32 CONTINUE
L.0046          WRITE(5,79) NPTS,II,IS
L.0047       79 FORMAT(3I3)
L.0048          DO 85 I = 1,NPTS
L.0049          READ(5,2) BX1(I),BX2(I),BX3(I),BX4(I),BX5(I),BX6(I),BX7(I),BX8(I),
L.0050         *BX9(I),BX10(I),BX14(I)
L.0051       21 FORMAT(1X,2F6.3,2X,1F7.3,7X,3F7.3)
L.0052        2 FORMAT(2F6.2,1F6.3,2F6.2,8F6.3)
L.0053          PRIO1 = BX1(I)
L.0054          P41 = BX2(I)
L.0055          T7 = BX3(I)
L.0056          SECO = BX4(I)
L.0057          P42 = BX5(I)
L.0058          T8 = BX6(I)
L.0059          P2 = BX7(I)
L.0060          PAP = BX8(I)
L.0061          T1  = BX9(I)
L.0062          T2  = BX10(I)
L.0063          COR = BX14(I)
L.0064          ROTO2 = SECO
L.0065          SECO = SECO * COR
L.0066          TERO = 0.5 * (T1 + T2)
L.0067          BX12(I) = TERO
L.0068          DPAP = (PAP - TERO)/332.1
L.0069          DPAPW = DPAP *27700.
L.0070          BX15(I) = DPAPW
L.0071          IF(T7 .LE.0.0) GO TO 23
L.0072          IF(PRIO1.LT.0.0) GO TO 19
L.0073          PP  = DPAP + PBAR
L.0074          P0 = PRIO1
L.0075          P2 = P0 + PBAR
L.0076          BX11(I) = PPP/P0
L.0077          BX13(I) = P0
L.0078          XNV = T7
L.0079          XNVW = T8
L.0080          T41 = P41 + PBAR
```

Figure B-1. Data Reduction Coding (Contd)

Reproduced from best available copy.

```
      T7 = 611.61 - (44.36 * XTV)
      PRIO1 = PRIO1 * 0.254
      P42 = P42 + PBAR
      T8 = 611.61 - (44.36 * XTTV)
      A = (530./14.7) * P41/T7
      SQA = SQRT(A)
      B = SQA * PRIO1
C---------INPUT = RHO(0) * (Q/60.) = 1.249 * B = C =----------------
      C = 1.249 * B
      XMACH = 5. ** 0.5 * (((P0/PPE) ** 0.2857 - 1.) ** 0.5)
      TS = T7/(1. + 0.2 * XMACH ** 2.)
      VP = XMACH * 49. * TS ** 0.5
      XMTHEO = VP * AP * PBAR * 28.966/(1545. * TS)
      CD = C/XMTHEO
      CD = CD/1000.
      D = (530./14.7) * P42/T8
      SQD = SQRT(D)
      E = SQD * SECO
      F = 1.249 * E
      XMU = 0.00018
      RE = XL * VP/XMU
      DOT1 = F/C
      BX16(I) = DOT1
      DOT2 = F + C
      DOT3 = DOT2/C
      DOT4 = DOT3/XD
   30 CONTINUE
      WRITE(6,20) P0,P41,T7,B,C,VP,TS,CD,
     * DOT2,P42,T8,DPAPE,F,DOT1,DOT2,DOT3,DOT4
   20 FORMAT(1X,1F6.1,1X,1F6.2,2F6.1,3X,1F5.1,1X,1F6.1,1X,1F10.3,1X
     *1F5.3,1X,
     *1F5.1,1X
     *1F6.2,1X,1F5.1,1F5.1,3X,1F5.1,
     *1X,1F5.2,2X,1F5.1,1X,1F5.2,3X,1F6.4)
   85 CONTINUE
      WRITE(6,12)
   12 FORMAT(//,10X,'EXPERIMENTAL DATA INPUT REQ.FOR COMPUTER',//)
      WRITE(6,9) (HEAD(I),I=1,18)
   90 FORMAT(10X,'COLUMN 8(PPE/P0),COLUMN 11 (AVG. T1 + T2) COMPUTED',2X,
     *,'NOT REQ. DATA INPUT')
```

Figure B-1. Data Reduction Coding (Contd)

Reproduced from best available copy.

```
L.0121          WRITE(6,101)
L.0122      101 FORMAT(14X,'D(IN.)',14X,'X(IN.)',16X,'PBAR',1PX,'DO')
L.0123          SM = (BX15(IL) -BX15(IS))/(BX16(IL) - BX16(IS))
L.0124          SP = BX15(IL) - (SM * BX16(IL))
L.0125          XINT = -SP/SM
L.0126          WRITE(6,107) DIA,X,PBAR,DO,THETA,XINT
L.0127      107 FORMAT(3F20.2,1F20.3,2X,'THETA=',1F5.2,2X,'MS/MRIM=',1F5.2,///)
L.0128          WRITE(6,70) IL,IS
L.0129          WRITE(6,102)
L.0130      102 FORMAT(15X,'PRIMARY',44X,'SECONDARY')
L.0131          WRITE(6,103)
L.0132      103 FORMAT(1X,26('-'),2X,91('-'),//)
L.0133          WRITE(6,104)
L.0134      104 FORMAT(66X,'PPI/PO',33X,'T',8X,'CON')
L.0135          WRITE(6,105)
L.0136      105 FORMAT(2X,'ROTO(%)',2X,'P41(PSIG)',1X,'T7(MV)',2X,'ROTO(%)',2X,
L.0137         *'P42(PSIG)',1X,'T8(MV)',1X,'P0(PSIG)',11X,'PAP(MV)',5X,'T(1)',
L.0138         *5X,'T(2)')
L.0139          DO 83 I = 1,NPTS
L.0140          WRITE(6,60) BX1(I),BX2(I),BX3(I),BX4(I),BX5(I),BX6(I),BX7(I),
L.0141         *BX11(I),BX8(I),BX9(I),BX10(I),BX12(I),BX14(I)
L.0142       60 FORMAT(13F9.3)
L.0143       83 CONTINUE
L.0144          READ(5,200) NEND
L.0145      200 FORMAT(I2)
L.0146          IF(NEND.LT.0.0) GO TO 23
L.0147        5 STOP
L.0148          END
L.0149  /DATA
L.0070  END
L.0072  BEGIN
```

Reproduced from best available copy.

Figure B-1. Data Reduction Coding (Contd)

NOZZLE S/N LD1C,D=0.48 IN.,X=10.00 IN.,DC=8.33 IN., 03/30/73-7

XD 0.20833E 02 PBAR 0.14398E 02 AP 0.18096E 00

PRIMARY

SECONDARY

ROTO (°)	P (PSIA)	T (R)	Q (SCFM)	MP MLB/S	VP FT/SEC	RE	CD	ROTO (°)	P (PSIA)	T (R)	DPAP MIM	MS MLB/S	MS/MP	MP&MS	TOT/PP	TOT/PP/XD
35.0	16.12	532.2	9.3	11.6	133.0	0.295E 05	0.948	60.0	18.79	527.3	0.8	84.9	7.32	96.5	8.32	0.3994
35.0	16.12	532.1	9.3	11.6	133.0	0.296E 05	0.948	55.0	18.38	527.0	0.5	77.0	6.64	88.6	7.64	0.3666
35.0	16.13	532.1	9.3	11.6	133.0	0.296E 05	0.948	52.0	17.87	526.6	0.3	71.8	6.19	83.4	7.19	0.3451
35.0	16.13	532.1	9.3	11.6	133.0	0.296E 05	0.948	48.0	17.25	526.4	0.0	65.2	5.61	76.8	6.61	0.3175

EXPERIMENTAL DATA INPUT REQ.FOR COMPUTER

NOZZLE S/N LD1D,D=0.48 IN.,X=10.00 IN.,DC=8.33 IN., 03/30/73-7

D(IN.) 0.48 X(IN.) 10.00 PBAR 14.40 DQ 8.330 THETA=42.86 MS/MPINT= 5.47

2 3

PRIMARY

SECONDARY

ROTO(°)	P41(PSIG)	T7(MV)	ROTO(°)	P42(PSIG)	T8(MV)	PO(PSIG)	PPE/PO	PAP(MV)	Z(1)	Z(2)	Z	CDN
35.000	1.720	1.771	60.000	4.390	1.881	0.140	0.990	4.045	4.036	4.036	4.036	1.000
35.000	1.720	1.773	55.000	3.980	1.888	0.140	0.990	4.043	4.036	4.037	4.036	1.000
35.000	1.730	1.773	52.000	3.470	1.896	0.140	0.990	4.040	4.036	4.036	4.036	1.000
35.000	1.730	1.774	48.000	2.850	1.901	0.140	0.990	4.036	4.036	4.036	4.036	1.000

Figure B-2. Typical Data Input/Output